Disaccharide Topology Induces Slow Down in Local Water Dynamics

Ana Vila Verde[*,†,‡] and R. Kramer Campen[*,†]

FOM Institute AMOLF, 104 Science Park, 1098 XG Amsterdam, The Netherlands, and Centro de Física, Universidade do Minho, Campus de Gualtar, 4710-057 Braga, Portugal

E-mail: a.vilaverde@amolf.nl; k.campen@amolf.nl

Phone: +31-20-7547 100. Fax: +31-20-7547 290

[*]To whom correspondence should be addressed
[†]FOM Institute AMOLF
[‡]Universidade do Minho

Abstract

Molecular level insight into water structure and structural dynamics near proteins, lipids and nucleic acids is critical to the quantitative understanding of many biophysical processes. Unfortunately, understanding hydration and hydration dynamics around such large molecules is challenging because of the necessity of deconvoluting the effects of topography and chemical heterogeneity. Here we study, via classical all atom simulation, water structure and structural dynamics around two biologically relevant solutes large enough to have significant chemical and topological heterogeneity but small enough to be computationally tractable: the disaccharides Kojibiose and Trehalose. We find both molecules to be strongly amphiphilic (as quantified from normalized local density fluctuations) and to induce nonuniform local slowdown in water translational and rotational motion. Detailed analysis of the rotational slowdown shows that while the rotational mechanism is similar to that previously identified in other aqueous systems by Laage, Hynes and coworkers, two novel characteristics are observed: broadening of the transition state during hydrogen bond exchange (water rotation) and a subpopulation of water for which rotation is slowed because of hindered access of the new accepting water molecule to the transition state. Both of these characteristics are expected to be generic features of water rotation around larger biomolecules and, taken together, emphasize the difficulty in transferring insight into water rotation around small molecules to much larger amphiphilic solutes.

Introduction

Because the chemistry of life occurs in an aqueous environment, mechanistic insight into life processes requires understanding how biomolecules interact with water. A growing number of studies have illustrated that for a variety of biological processes continuum treatments of water are not appropriate because the molecular nature of water plays a critical role. For example, potential-sensing transmembrane proteins appear to require water molecules to screen charged residues within the hydrophobic membrane interior[1–4] and accounting for the anisotropic diffusion of protons near

membranes requires a population of ordered water molecules at the membrane/water interface.[5–7] Water structure, both in bulk and around solutes, is known to evolve on picosecond timescales (see, for example, recent reviews by Bakker, and Tokmakoff and coworkers[8,9]). Because a variety of important biochemical processes – e.g. dewetting of hydrophobic pockets during ligand docking and hydrophobic collapse during protein folding[10–12] – occur on this timescale, it is clear that understanding the molecular nature of water in many biological systems requires insight into both time-averaged structure and structural dynamics.

A variety of studies of solvation have been done on large biomolecular systems. These studies have demonstrated that local water structure and structural dynamics are strongly related to both solute chemistry (i.e. mixture of nominally hydrophobic and hydrophilic groups) and topology (i.e. surface roughness).[13] For example, hydrophobic collapse appears to play an important role in some protein folding events but the extent of dewetting has been shown to correlate with angstrom scale chemistry and topology.[11,12,14] However, deconvoluting these effects in large molecules is challenging.

In a reductionist spirit, a variety of workers have investigated water structure around nominally hydrophilic, hydrophobic and amphiphilic small solutes. Computational and experimental studies with hydrophilic solutes of varying size have generated qualitatively similar results: time averaged water structure and free energy of solvation can be rationalized accounting for the strength and manner (i.e. is the solute an H-bond acceptor or donor) of water/solute interaction.[8,15,16] From a structural point of view, regardless of solute size, simulations of water near idealized hydrophobic solutes and surfaces (mathematically smooth excluded volume particles and surfaces) reveal both an interfacial water density gap and an aqueous interface characterizable by density fluctuations.[17–19] X-ray and neutron studies have observed this density gap for the water / hydrophobic self-assembled monolayer interface.[20–22] In a series of more recent classical MD studies by Garde and coworkers of SPC/E water meeting self-assembled monolayers (SAMS) of various defined composition it was demonstrated that an interfacial density gap is not a good metric of hydrophobicity: there was no correlation between density gap and experimentally measured contact angle.

In contrast, the size of interfacial SPC/E water density fluctuations appears to map perfectly to contact angle measurements.[23–25] This suggests, then, that the most accurate metric to understand hydrophobicity on small length scales is as induced local density fluctuations in neighboring water.

Because individual water molecules cannot move without breaking and reforming hydrogen bonds, to develop a molecular scale understanding of the structural dynamics of water we require molecular scale understanding of hydrogen bond dynamics. In a recent series of simulation papers Laage, Hynes and coworkers have demonstrated that rotation of SPC/E water is best understood as the result of individual water molecules rotating, and individual hydrogen bonds breaking, via fast ($<$ 200 fs) large amplitude angular jumps.[26–28] In their description this large amplitude angular jump passes through an unstable (lifetime less than 200 fs), higher energy intermediate – a bifurcated hydrogen bond. Both the presence of the large amplitude angular jump and the instability of the bifurcated intermediate have been found to be consistent with ultrafast time resolved infrared and two dimensional infrared spectroscopies.[29–31]

Armed with a microscopic picture describing structural dynamics, i.e. hydrogen bond dynamics, in SPC/E water in the bulk, we can ask how it changes around solutes. Water rotational dynamics has been studied in salt solutions and around various types of amphiphilic molecules using ultrafast time resolved IR polarization anisotropy, two dimensional IR spectroscopy and NMR.[8,32–40] These studies paint a picture in which water rotation is slowed with respect to bulk by both nominally hydrophobic and hydrophilic solutes. In simulations of H-bond exchange around both hydrophilic and hydrophobic small solutes Laage, Hynes and coworkers have quantitatively described slowdowns from bulk hydrogen bond exchange as the result of two effects.[41–43] For hydrophilic solutes – those that accept hydrogen bonds from water – the free energy of hydrogen bond stretching (the first step in the exchange mechanism) may differ from that in bulk. For both hydrophilic and hydrophobic solutes the geometry of the solute may create a transition state excluded volume effect: approach of the new acceptor may be limited by the solute.

To help bridge the gap between studies of water structure and dynamics around large biomolecules and work around smaller solutes we would like a solute that is large enough to show

some of the features of large biomolecular hydration – amphiphilicity (i.e. chemical heterogeneity) and variable topology – but still small enough to make detailed analysis computationally tractable and that, due to its internal structure, makes it possible to straightforwardly distinguish chemical and topological effects. Here we meet these requirements by studying the structure and structural dynamics of SPC/E water around the disaccharides Kojibiose (α-D-glucose(1$\rightarrow$2)α-D-glucose) and Trehalose (α-D-glucose(1$\rightarrow$1)α-D-glucose) (see Figure 1) using classical, all atom molecular dynamics simulation.

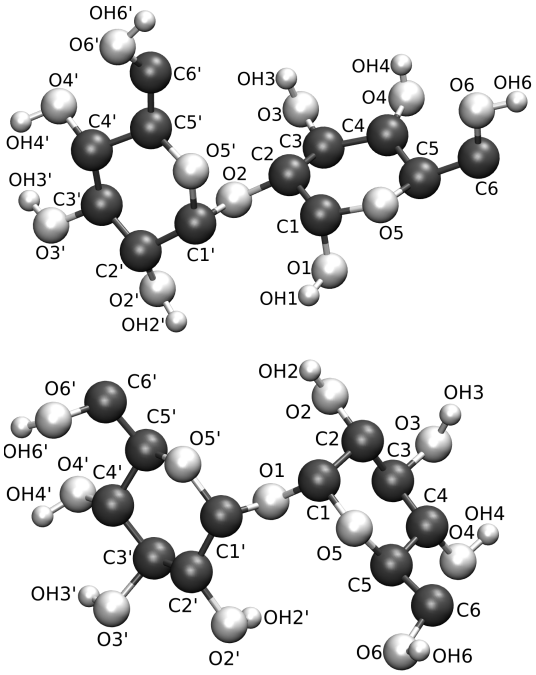

Figure 1: Structure of Kojibiose (top molecule), α-D-glucose(1$\rightarrow$2)α-D-glucose and Trehalose (bottom molecule), α-D-glucose(1$\rightarrow$1)α-D-glucose. The orientation of each monosaccharide relative to its neighbor is defined by two dihedrals: ϕ = O5$'$-C1$'$-On-Cn and ψ=C1$'$-On-Cn-C(n+1).

Disaccharides clearly meet the first requirement. They are expected to be amphiphilic because each molecule has oxygens of different polarity – the ether oxygens are less electronegative than those in hydroxyl groups. Because the equilibrium orientation of the two monosaccharides in each molecule differs (i.e. each populates different portions of a ϕ/ψ plot, see Figure 1 for angle definitions), we also expect that each sugar should confine water between the two rings differently: there should be a population of water molecules in the first solvation shell that feels the effects

of solute topology differently in Kojibiose than in Trehalose. Systems containing fully solvated disaccharides are also small enough to allow detailed computational analysis (thus satisfying the second requirement). Finally, disaccharides satisfy the third requirement, allow the deconvolution of chemical and topological effects, in two ways. By comparing water structure around the chemically identical O2′ and O4′ for a single molecule we can presumably understand the effect, if any, of hydroxyl group position on a glycosidic ring on local water structure. Similarly, because for each disaccharide the equilibrium position of the two rings relative to each other is different, comparison of water structure and structural dynamics around chemically equivalent oxygens on each disaccharide can be expected to give insight into the effect of the relative conformation of the two rings on water.

While trying to understand water structure and structural dynamics around these disaccharides is useful for the potential insight it offers into biomolecular hydration generally, it is also of interest in its specifics. A number of prior studies have shown that Trehalose is synthesized by a variety of microorganisms as protection against extremes in temperature and desiccation while others have shown that Trehalose is, possibly for similar reasons, useful as an additive in various frozen foods.[44–47] A number of hypotheses have been advanced for this protection effect: Trehalose more effectively interacts with membrane polar groups than water (effectively displacing water and preserving membrane fluidity at subfreezing temperatures); concentrated solutions of Trehalose have properties (e.g. a lower glass transition temperature) that inhibit freezing and differ from those of concentrated solutions of other sugars; the manner in which individual Trehalose molecules interact with water is sufficiently different from other sugars so as to lower the freezing temperatures of relatively large volumes of water per solute molecule. By characterizing sugar amphiphilicity and local water structure and structural dynamics around Trehalose and Kojibiose we can conclusively address the last of these proposed mechanisms.

A variety of authors have studied, both experimentally and computationally, water structure and dynamics near several disaccharides. For reasons sketched above most of that work involves the comparison of Trehalose and other molecules. The majority of experimental studies of these sys-

tems have either been thermodynamic (calorimetry), time averaged structural (e.g. neutron diffraction or scattering) or studies of how sugars perturb the time averaged spectral response of the OH stretch of water (e.g. inelastic neutron and spontaneous Raman scattering).[48–56] Concurrently, THz absorption and inelastic light scattering spectroscopies have also been employed to investigate slowdown of water structural dynamics as a function of sugar type.[57–59] In the last twenty years there have also been a number of computational studies of water structure and structural dynamics near various disaccharides (often including Trehalose and focussed on the influence of water on sugar properties).[60–67] In general, these studies paint a picture in which water near Trehalose is more strongly hydrogen bonded than that near other sugars and the effect of Trehalose on local water dynamics more pronounced. Both types of work have, in general, not provided the sort of detailed insight that seems potentially useful. For example, there are no studies that quantify changes in local hydrophobicity around disaccharides nor are there studies which locally map dynamic observables (e.g. rotational anisotropy and mean square displacement of water near particular hydrogens) and connect these dynamic observables to local sugar structure.

Here, then, we use the SPC/E water model to map a variety of water properties around Kojibiose and Trehalose. We opt for this model because, as mentioned above, it adequately captures the quantities of interest: water density fluctuations and rotational dynamics.

We find that metrics of local hydrophobicity suggest that Kojibiose and Trehalose are strongly amphiphilic, that both slow the rotational and translational motion of water in their hydration shells and that the specifics of these slowing downs correlate with hydrophobicity: the most hydrophobic locations on each sugar molecule appear to induce the largest slow down in neighboring water dynamics. Performing an analysis similar to that of Laage, Hynes and coworkers we further find that trends in time averaged geometric parameters (distances and angles) near hydrogen bond exchange events do not correlate with differences in dynamic behavior: slowdown of water dynamics in the sugar solvation shell must be the result of changes in rotation rate, not mechanism.

Analysis of the rotation mechanism makes clear that the water rotation around sugars (in general) slows relative to rotation in bulk because of transition state excluded volume effects; the

slowdown is smaller than that predicted from transition state excluded volume because of increased accessible transition state geometries. For water molecules that donate hydrogen bonds to a sugar oxygen, rotational dynamics further slow because of enthalpic and entropic differences between the water→sugar (where X→Y indicates that species X donates a hydrogen bond to species Y) hydrogen bonded state and water in the bulk. These effects are strongly a function of sugar and particular water subpopulation. Finally, the slowest rotating subpopulation of waters, that near the glycosidic linkage in Trehalose and hydrogen bonded to the sugar, are also strongly influenced by an increase in the free energy cost to bring a new accepting water molecule close to the initial pair. Our results make clear that this enhanced free energy barrier to rotation is the result of Trehalose's surface topology.

Some of the phenomena we observe associated with the slowdown of water rotational dynamics around Kojibiose and Trehalose – namely the broadening of the transition state of hydrogen bond exchange for all water molecules in the sugar hydration shells and the extreme slowdown of water rotation near the glycosidic linkage of Trehalose induced by solute topology – have not been described before. As noted above, relative to other biomolecules, disaccharides only weakly perturb the local hydrogen bond environment of water in the bulk and have muted surface roughness. We therefore expect that both effects we observe should be significant for biomolecular hydration in general.

Methods

In this study we performed all-atom molecular dynamics simulations of Kojibiose and Trehalose in water using the molecular dynamics package NAMD, the SPC/E model for water and the GLYCAM 06.b force field for the sugars.[68–70] Trajectories were visualized and analyzed using the package VMD–Visual Molecular dynamics.[71] Van der Waals (VdW) interactions were smoothly set to zero between 10 and 12 Å. Electrostatic interactions were calculated directly for distances below 12 Å and using the Particle Mesh Ewald method with a grid spacing of 1 Å for larger

distances. A modified Verlet algorithm was used for integration. Van der Waals forces were calculated every 2 fs, electrostatic forces every 4 fs and the remaining forces every 1 fs. The SHAKE algorithm was used to fix the length of all bonds involving hydrogen. The starting configurations for solvated sugars were obtained by surrounding each sugar with 10 Å of water in each direction using the biomolecule builder available in the GLYCAM website and equilibrating them at a constant pressure of 1 atm and temperature of 300 K for 10 ns. The initial configuration for simulations of water in the bulk was created using the water box feature implemented in VMD to generate a simulation box containing 954 water molecules and equilibrating it for 2 ns at 1 atm and 300 K. Production runs for all systems were performed subsequently in the microcanonical ensemble for 3 ns, with configurations saved every 2 fs. The average temperature for simulations of water in bulk was 300.7 K, for the Trehalose solution was 299.7 K and for the Kojibiose solution was 304.0 K. In this small temperature range the dynamics of water rotation near small solutes has been shown not to vary significantly[72] so results can be directly compared between simulations. Following our prior work in vacuum,[73] we verified that disaccharide configurational phase-space is well explored in these simulations by comparing the distributions of the configurations of the hydroxyl groups, the rings (chair or boat configuration) and the two dihedral angles defining the disaccharide linkage with the corresponding distributions obtained from replica exchange molecular dynamics simulations of solvated Kojibiose and Trehalose between 300 K and 735 K. Results (not shown) indicate that molecular dynamics simulations at 300 K sample the same configurations as those accessed by the replica at the same temperature during the replica exchange simulations.

Results and Discussion

To this point we have asserted that both Kojibiose and Trehalose are amphiphilic by invoking chemical intuition: ether oxygens are less polar than those in hydroxyl groups. To quantify the amphiphilicity of these molecules a local metric of hydrophobicity is required. Theoretical approaches and molecular simulation have clarified that the free energy of hydration for small excluded volume

(ideal hydrophobic) solutes, is principally entropic: excluded volume solutes are accommodated by deformation, but not breakage, of liquid water's H-bond network. In contrast, in the hydration of larger ideal solutes hydrogen bonds are broken so the enthalpic contribution to the free energy of hydration is significant. For these larger ideal solutes, water dewets the solute/water interface and interfacial water is characterized by large density fluctuations.[17,18,74–77] Both integral equation approaches and molecular simulation suggest that for real larger hydropobic solutes or hydrophobic surfaces electrostatic or van der Waals interactions as well as surface curvature effects may act to minimize dewetting but that density fluctuations persist.[19,78,79] In a recent study by Garde and coworkers these ideas have been extended to microscopically characterize the hydrophobicity of a number of self-assembled monolayers.[23] Because these systems allow straightforward macroscopic experimental description of hydrophobicity, by measurement of contact angles, they were able to show that metrics that capture interfacial density fluctuations in the simulations have a linear relationship with experimentally quantified hydrophobicity. Subsequently several of the same authors demonstrated in idealized SAMs that hydrophobicity can be context dependent (adding a CH_3 group in the middle of an otherwise OH terminated monolayer produces a dramatically different effect than adding an OH group in the middle of an otherwise CH_3 terminated monolayer) and that using a local metric of hydrophobicity that quantifies averaged density fluctuations offers a perspective on amino acid hydrophobicity more useful than conventional, context independent, residue based classification.[24]

Inspired by this work we mapped local hydrophobicity around each sugar by calculating the normalized fluctuation in hydration number within 3.5 Å of each oxygen in both Kojibiose and Trehalose. For comparison we also present the average hydration number in the same volume. Because of the proximity of adjacent functional groups some water molecules will belong to more than one site and will be doubly counted. This simply mirrors the fact that local hydrophobicity reflects both the character of the functional groups considered *and* their surroundings. Note that the volume available for water molecules near each oxygen differs from site to site because of differences in local molecular geometry. For this reason hydration numbers do not reflect the local

water density near each sugar oxygen. In contrast, the normalized fluctuations in hydration number map directly to relative density fluctuations because the volume term cancels out. The results of this analysis are shown in Table 1. Two trends are clear from inspection. Firstly, hydrophilicity decreases as one moves from hydroxyl oxygens to ether oxygens within a monosaccharide (O5 or O5′ within either Kojibiose or Trehalose) to the linking oxygens (oxygen in the glycosidic linkage, O1 in Trehalose and O2 in Kojibiose). Secondly, whereas the O5 or O5′ still have hydrophilic character, the linking oxygens of Trehalose and Kojibiose are hydrophobic, the linking oxygen of Trehalose being the most hydrophobic of the two. These conclusions are supported by an analysis of hydrogen bond frequency. Water does not form hydrogen bonds (except where otherwise noted, hydrogen bonds are defined geometrically as O-H$\cdots$O angle $>140^{\circ}$ and O$\cdots$O distance <3.5 Å) with the linking oxygen of Trehalose and forms few hydrogen bonds (< 13% of the time) with the linking oxygen of Kojibiose. In each case water within 3.5 Å of either linking oxygen may hydrogen bond to a neighboring more polar oxygen (e.g. O2 and O2' in the case of Trehalose, see Figure 1B). Also note that water near O5 or O5′ in either molecule behaves differently than water near the linking oxygens. These oxygens accept hydrogen bonds from water $\approx 50\%$ of the time.

Table 1: Fluctuation of average number of waters (average number of waters) within 3.5 Å of a sugar oxygen[a].

	Trehalose	**Kojibiose**
Linking Oxygen	0.76 (0.6)	0.46 (1.04)
O5	0.37 (1.4)	0.38 (1.9)
O5′	0.37 (1.4)	0.38 (1.4)
All Other Oxygens	0.26 (3.0)	0.27 (3.1)
Bulk water	0.19 (6.1)	

a The linking oxygen is O1 in Trehalose and O2 in Kojibiose (see Figure 1). Normalized density fluctuations in local water density are calculated as $\left(\langle N^2\rangle - \langle N\rangle^2\right)/\langle N\rangle$. For comparison, the number of water molecules and the density fluctuations in a sphere of radius 3.5 Å in water in the bulk are also given.

Armed with the knowledge that both molecules are amphiphiles, we explored the translational dynamics of individual water molecules in the sugar solvation shell by calculating water mean square displacement (MSD). Our approach differs from that of prior work,[64,67] in calculating *lo-*

cal translation dynamics: we calculate independent values of the MSD for water initially (i.e. at time = 0) within 3.5 Å of each sugar oxygen. The results of this analysis are shown in Figure 2. Comparison of Figure 2 and Table 1 makes clear that slowdown of water translational motion

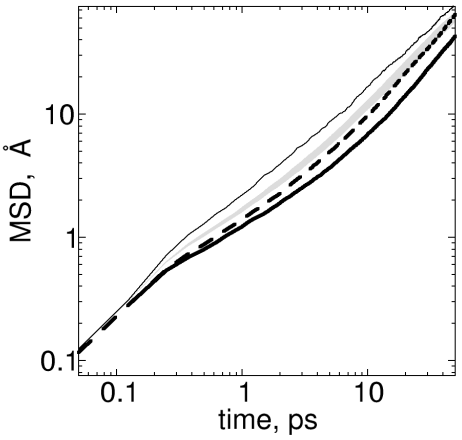

Figure 2: Mean square displacement for water molecules initially within 3.5 Å of sugar oxygens. The thin black line is the calculated MSD for the SPC/E water model in water in the bulk. The slowest translating water molecules (thick black line) are those near the linking oxygen of Trehalose (O1 in Figure 1B) while the next slowest (the dashed black line) are those near the linking oxygen of Kojibiose (O2 in Figure 1A). The MSD of all other water molecules around both sugars (the light grey band) plots still closer to bulk.

correlates with local hydrophobicity: the most hydrophobic locations on the solutes also have the slowest translational dynamics of neighboring water molecules.

In water solvating both sugars and proteins prior studies have found that rotational and translational motion are decoupled.[64,80,81] Motivated by this observed decoupling we also characterized the effect of either Kojibiose or Trehalose on water rotational motion by calculating a rotational correlation function for water initially within 3.5 Å of each sugar oxygen. Following prior authors,[26,28,41,43] we quantify rotational dynamics by calculating the rotational anisotropy (R),

$$R(\tau) = \frac{2}{5} \langle P_2 \left| \vec{u}(0) \cdot \vec{u}(\tau) \right| \rangle \tag{1}$$

in which P_2 is the second order Legendre polynomial and $\vec{u}$ is the unit vector describing the orien-

tation of an OH group at time τ. Rotational anisotropies are conventionally reported including the factor of $2/5$ so that they match the observable monitored in pump-probe spectroscopy. This factor implies that the maximum value of $R(\tau)$ is 0.4, not 1 as is common for autocorrelation functions. The results of this analysis for water populations initially (at $\tau = 0$) within 3.5 Å of individual sugar oxygens are shown in Figure 3 (top panel). Clearly differences in rotational dynamics between wa-

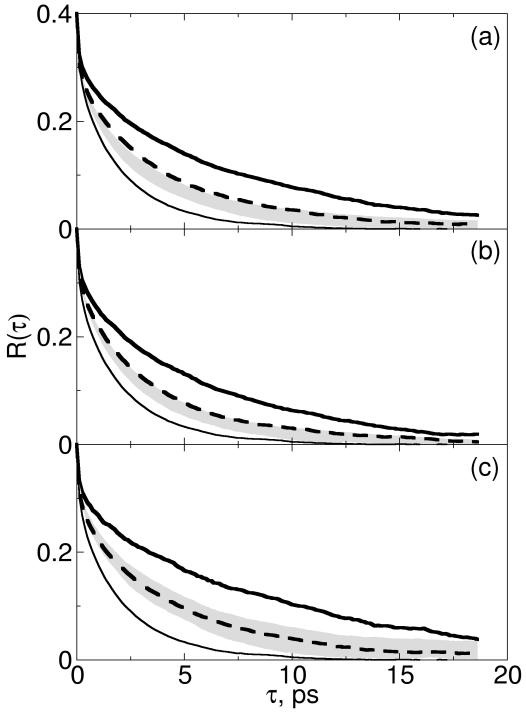

Figure 3: Rotational anisotropy of waters which at time $\tau = 0$ are within 3.5 Å of a sugar oxygen. The thick black line indicates water around the linking oxygen of Trehalose, the dashed black line water around the linking oxygen of Kojibiose and the light grey band water around each of the other sugar oxygens. The thin black line is the rotational anisotropy of water in the bulk. The top plot (a) shows the calculated rotational anisotropies for all water molecules in the sugar hydration shell, the middle one (b) the subpopulation of water molecules that at $\tau = 0$ are hydrogen bonded to other waters and the bottom one (c) the same quantity for those waters that at $\tau = 0$ donate hydrogen bonds to sugar oxygens.

ter subpopulations correlate with differences in MSD and hydrophobicity: water near the linking oxygen of Trehalose has the most slowed rotational motion, followed by water near the linking oxygen of Kojibiose, followed by water near all other sugar oxygens. The middle and bottom pan-

els of Figure 3 are decompositions of the results shown in the top panel. In the middle panel the rotational anisotropy of OH groups initially within 3.5 Å of a sugar oxygen and H-bonded to other waters (these are hereafter termed water→water interactions) is shown, in the bottom panel the rotational anisotropy of water initially within 3.5 Å of a sugar oxygen and donating an H-bond to a (possibly different) sugar oxygen (hereafter water→sugar interactions) is illustrated. Comparison of the top and bottom panels of Figure 3 highlights that the slowest rotating population of waters in either system are those initially within 3.5 Å of the Trehalose linking oxygen and hydrogen bonded to a sugar oxygen. We quantified these qualitative impressions by fitting single exponentials to the data shown in Figure 3 and extracting characteristic time constants (shown in Table 2).[82] Reference

Table 2: Rotational anisotropy decay times extracted from single exponential fits to the data in Figure 3[a].

	Population	**Trehalose**	**Kojibiose**
Linking Oxygen	W→W	6.7 (0.5)	4.2 (0.5)
	W→S	10.2 (0.5)	5.1 (0.5)
Other Oxygens	W→W	3.5 (0.4)	3.4 (0.3)
	W→S	5.3 (1.3)	4.6 (0.9)

a The characteristic rotational time of water in the bulk following this protocol (for the SPC/E water model) is 2.3 ± 0.5 ps. The quantities in parentheses are the standard deviation of the average (for other oxygens) or the uncertainty (for the linking oxygen). The latter is estimated by fitting exponential curves to different subsets of the data and taking the largest difference between the time constants obtained for each water population.

to Table 2 clearly shows that the slowest rotating population of water molecules are those initially within 3.5 Å of the linking oxygen of Trehalose (these rotate $\approx 5\times$ more slowly than water in the bulk). It also highlights that, as for water translational dynamics, a slowdown in rotation appears to map to local hydrophobicity: water near the most hydrophobic sugar oxygen, the linking oxygen of Trehalose, rotates most slowly, while water near the second most hydrophobic sugar oxygen, the linking oxygen of Kojibiose, has the next slowest rotation. It is thus clear that in general water is slowed within the solvation shell of disaccharides and that this slowdown is dramatically nonuniform. The fitted time constants for each water subpopulation for both sugars are shown in the supporting information.

The simplest explanation for the general slowdown of water structural dynamics near sugars and the correlation of local hydrophobicity and structural dynamics is that the thermodynamics of hydrogen bonding changes for water molecules that are either near or donate hydrogen bonds to sugars. If, for example, hydrogen bonds donated by water molecules to sugar oxygens were energetically favorable relative to those donated to other water molecules we might expect that the resulting structural dynamics would be slowed. We tested this scenario by examining the time averaged geometric parameters describing hydrogen bonding: a stronger hydrogen bond would be expected to differ geometrically from a weaker. The largest difference in water dynamics we observe is between water near the linking oxygen of Trehalose, the linking oxygen of Kojibiose and in bulk. Thus we test the possibility of differences in hydrogen bond strength between these populations by calculating the normalized probability distribution functions of O$\cdots$O distance and O-H$\cdots$O angle for hydrogen bonded pairs in these subpopulations (see Figure 4).[83] Several qualitative points are apparent from inspection of this data. Firstly, by these metrics waters hydrogen bonded to other waters within 3.5 Å of either sugar are quantitatively indistinguishable from each other and from water in bulk. Secondly for water molecules hydrogen bonded to sugar functional groups any slight differences between water$\rightarrow$sugar and water in the bulk tend in an opposite direction than the dynamics: if anything water around Kojibiose has slightly more strained hydrogen bonds (longer O$\cdots$O distances and more acute OH$\cdots$O angles) than water near Trehalose, opposite to the trends in rotational and translational slowdown (see Figure 2, Figure 3 and Table 2). If hydrogen bond strength is similar for all populations of water molecules, differences in water dynamics may be the result of changes in rotation mechanism: perhaps water rotates through a different mechanism when it is near a disaccharide than in bulk. As alluded to above, prior work by Laage and Hynes on the mechanism of water rotation (i.e. hydrogen bond breaking) in water in the bulk and water around small solutes has developed both a qualitative picture and a quantitative analytical transition state formalism that allows the description of the free energy of hydrogen bond exchange (or equivalently, water rotation).[26–28,41–43] In their description (see Figure 5) the following sequence of events is associated with large amplitude water rotation / hydrogen bond

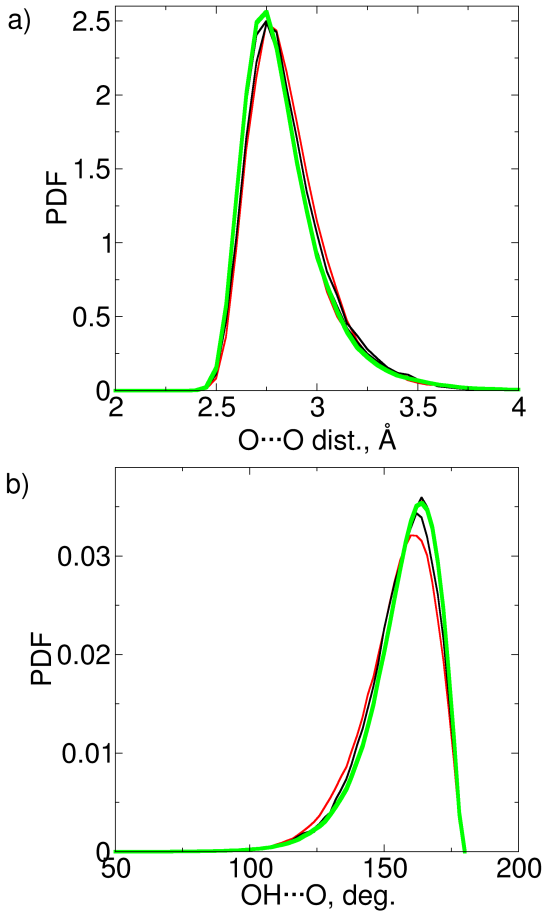

Figure 4: Probability distribution function of a) O···O distance and b) OH···O angle obtained using the SPC/E water model for water→water and water→sugar hydrogen bonds formed by molecules initially within 3.5 Å of the linking oxygen of Trehalose (black), Kojibiose (red) and in SPC/E water in the bulk (green). The statistics for water→water hydrogen bonds in either sugar's hydration shell are indistinguishable from water in the bulk and lie behind the green curve; the visible red and black curves are water→sugar hydrogen bonds.

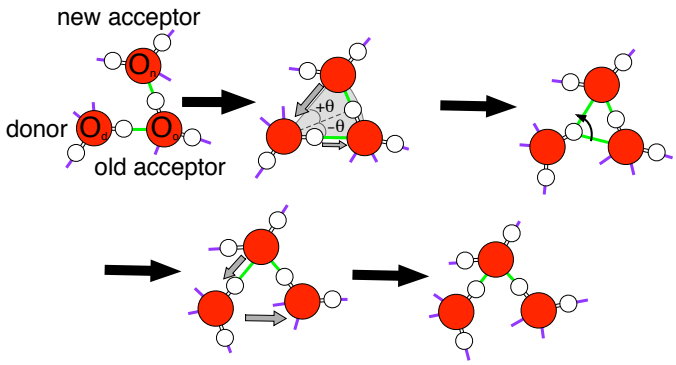

Figure 5: Angular jump mechanism of hydrogen bond exchange after Laage and Hynes.[28] In what follows we calculate the distance both between the hydrogen bond donor and old hydrogen bond acceptor ($O_d \cdots O_o$) and donor and the new hydrogen bond acceptor ($O_d \cdots O_n$) as well as the jump angle (θ). θ is defined to be zero at the bisector of the $\angle O_o - O_d - O_n$ angle.

exchange. Initially one water donates a hydrogen bond to another. At some point, due to fluctuations in the system, the $O_d \cdots O_o$ distance begins to expand while the distance between a water molecule hydrogen bonded to O_o but not interacting with O_d (i.e. O_n) and O_d begins to decrease, O_o is overcoordinated and O_n is under coordinated. As these coupled translations continue, at some point the $O_d \cdots O_o$ and $O_d \cdots O_n$ distances are equal. At this point the O_d group undergoes a large amplitude, rapid, angular jump. After the jump the $O_d \cdots O_o$ distance continues to increase and the $O_d \cdots O_n$ to decrease.

This hydrogen bond exchange mechanism dominates in bulk, and differs from the proposed mechanisms of exchange of hydrogen bond donor and acceptor in water dimers. Exchange in dimers was studied using both classical water models (of the TIP family) and ab initio calculations, with conflicting results: whereas from classical simulations the transition state for the donor-acceptor exchange process is an anti-aligned dipole,[84] ab initio calculations indicate it is a bifurcated hydrogen bond structure.[85] We note that the origin of this discrepancy between classical and quantum simulations is not obvious because the classical simulations report free energies as a function of configuration but the ab initio ones report only potential energies. Neither the anti-aligned dipole configuration nor the bifurcated hydrogen bond structure characteristic of donor-acceptor exchange in dimers have been observed for hydrogen bond exchange in bulk using the SPC/E water model.

We investigated whether large amplitude angular jumps are present in water near sugars in the following manner. 1.) We identified large amplitude angular jumps relative to an external reference frame. 2.) We looked for the hydrogen bond acceptor associated with the rotating OH both before and after the jump. In this analysis, for reasons discussed further below and in the supporting information, we focus on strong hydrogen bonds, i.e. those with O-H$\cdots$O angle $>140^{\circ}$ and O$\cdots$O distance <3.1 Å. 3.) We calculated the angle θ between the projection of the donating hydroxyl group on the plane defined by O_d, O_o and O_n and the bisector of the angle formed by those three oxygens (θ is zero at the bisector of the O_o-O_d-O_n angle), the distance between the hydrogen bond donor and old acceptor ($O_d \cdots O_o$) and the distance between the hydrogen bond donor and new acceptor ($O_d \cdots O_n$) as illustrated in Figure 5. Time zero for the jump event was defined as the first configuration in which $\theta \geq 0$. After calculating these parameters for each jump event in each SPC/E water subpopulation – water in the bulk, water initially within 3.5 Å of each sugar oxygen and hydrogen bonded to other water, water initially within 3.5 Å of each sugar oxygen and hydrogen bonded to a sugar – we averaged the trajectories with respect to each geometric parameter for all waters in a given subpopulation. The results of this analysis for water $\rightarrow$ sugar hydrogen bonds for angles and distances are shown in Figure 6 and for water$\rightarrow$water interactions in Figure 7. The results for water$\rightarrow$sugar and water$\rightarrow$water hydrogen bond coordination are shown in the supporting information.

Several qualitative observations are apparent from inspection of these results. Firstly, the conceptual model of hydrogen bond exchange developed, and shown to be consistent with experiment, by Laage, Hynes and coworkers for SPC/E water in the bulk,[26–28] and SPC/E water around ions,[16] small hydrophobic solutes,[41] amino acids[43] and idealized hydrophobic surfaces[86] also applies for water near sugars. Inspection of the change in θ over a jump event ($\Delta\theta$) suggests that, in general, angle jump size is slightly less for water hydrogen bonded to sugars than for water in the bulk. However, changes in jump angle size do not correlate with changes in dynamics. For both Trehalose and Kojibiose water rotates most slowly near the linking oxygen but in Trehalose this population has a substantially larger jump angle than those waters near the ring oxygens (O5 and

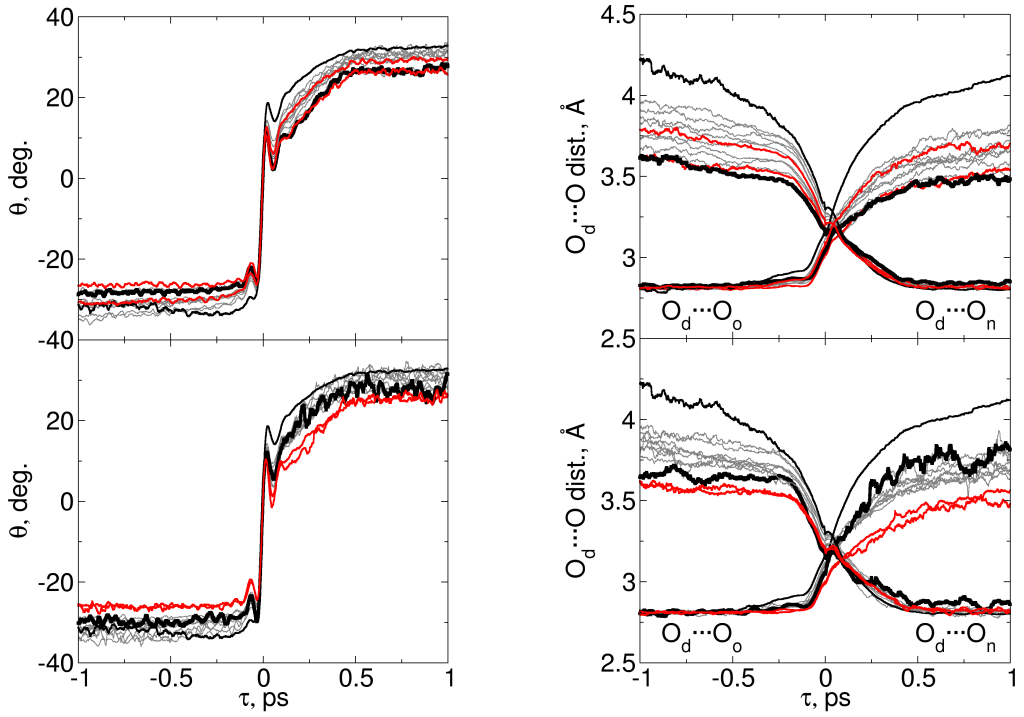

(a) (b)

Figure 6: Average change in hydrogen bond (a) exchange angle (θ) and (b) Oxygen/Oxygen distance near hydrogen bond exchange events for SPC/E water hydrogen bonded to sugar functional groups in Kojibiose (top panels) and Trehalose (bottom panels). The thick black lines are average values for water near the linking oxygen, the red lines average values for water near the ring oxygens (O5 and O5′), the grey lines average values for water near all other sugar oxygens and the thin black lines, on all panels, values for SPC/E water in the bulk. $O_d \cdots O_o$ distances are initially $\approx$ 2.8 Å and rapidly increase near 0 ps. $O_d \cdots O_n$ distances are initially 3.6 - 4.3 Å and rapidly decrease near 0 ps. The change in jump angle during hydrogen bond exchange for each water subpopulation ($\Delta\theta$) is tabulated in the supporting information.

O5′) whereas in Kojibiose it is similar.

Above, we have demonstrated that translational motion of water near sugars is perturbed relative to that in bulk (see Figure 2). Because the rotation of water involves two translation motions (the decrease of the $O_d \cdots O_n$ and the increase of the $O_d \cdots O_o$ distance) we might expect this translational slowdown to correlate with differences in the rotational mechanism. Inspection of Figure 6(b) makes clear that this is, in general terms, the case. For all subpopulations of water molecules near either sugar, decrease in the $O_d \cdots O_n$ before and increase in the $O_d \cdots O_o$ distance after the jump happens more slowly than in water in the bulk. However, similar to angular jump size, no correlation exists between these average distances around jump events and water slowdown between sugar populations. For example, for the Kojibiose/water system, water near the linking oxygen rotates more slowly than all other water populations. As is clear from Figure 6(b), this water enters and exits the transition state more slowly than all other water subpopulations around Kojibiose. In contrast, in the Trehalose/water system water around the linking oxygen once again rotates most slowly but now appears to arrive at a jump with rates similar to other waters and to leave the jump most rapidly. In summary it appears that, while the averaged $O_d \cdots O_o$ and $O_d \cdots O_n$ distances describing hydrogen bond exchange events for water→sugar hydrogen bonds differ from water in the bulk in ways consistent with the observed slowdown in water rotational and translation motion, differences in these parameters between water subpopulations around either sugar do not correlate with trends in MSD or rotational anisotropy.

Inspection of Figure 7 clarifies that for water→water interactions in the sugar hydration shell the change in θ, $O_d \cdots O_o$ and $O_d \cdots O_n$ near jump events differs very little from the behavior of these parameters in water in the bulk. Despite this essential similarity in water rotation mechanism, calculation of the MSD and rotational anisotropy highlights both that each subpopulation experiences slowed translation and rotation relative to water in the bulk and that there are significant dynamics differences between different populations in the sugar hydration shell (see Figure 2, Figure 3, Table 2 and supporting information). This lack of correlation between changes in the geometric parameters describing jump events as a water molecule moves from bulk to a water→water

interaction in the sugar hydration shell to a water→sugar interaction suggests that both the general slowdown of water rotation and translation relative to bulk in the sugar hydration shell and variability in water dynamics around Kojibiose and Trehalose are not the result of a different mechanism of water rotation near sugars than in the bulk, rather they must result from a change in rotation rate within the same mechanistic picture.

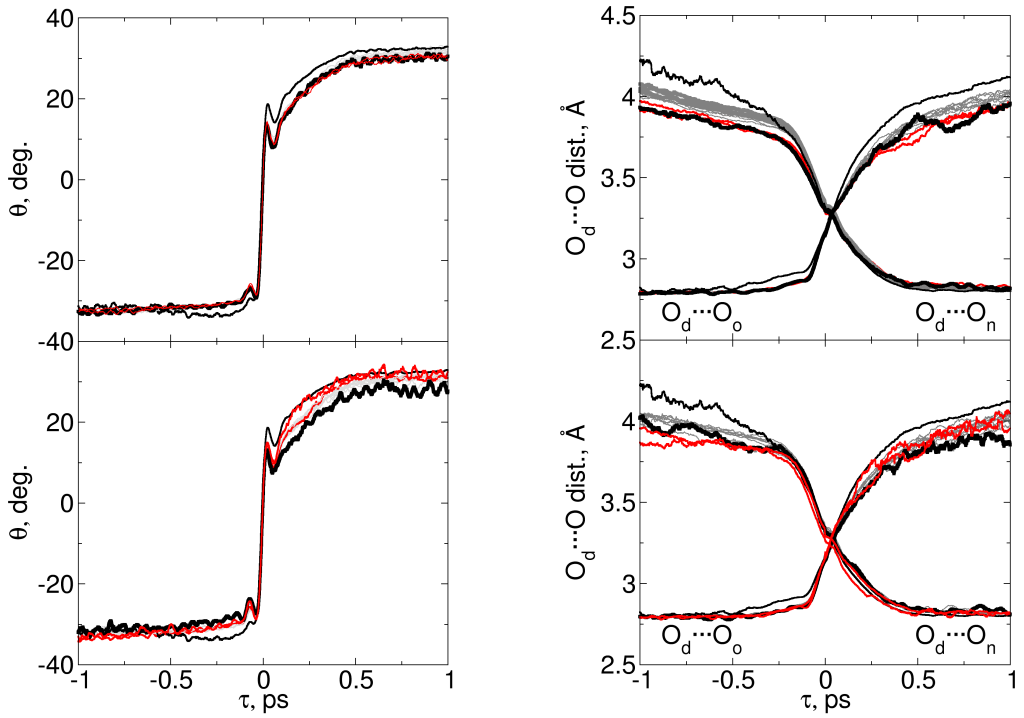

Figure 7: Average change in hydrogen bond (a) exchange angle (θ) and (b) Oxygen/Oxygen distance near hydrogen bond exchange events for water hydrogen bonded to waters and within 3.5 Å of sugar oxygens in Kojibiose (top panels) and Trehalose (bottom panels). See legend of Figure 6 for details.

To understand the origin of this decrease in rotation rate it is convenient to adopt the formalism which Laage, Hynes and coworkers first applied to SPC/E water in the bulk.[26,28] In their description, the characteristic reorientation time extracted from the fits to the rotational anisotropy (τ_r) reflects the loss of rotational correlation due to large amplitude angular jumps (that occur with a characteristic time τ_{ex}) and a diffusive reorientation that occurs in the interval between jumps

(i.e. the frame reorientation that occurs with a characteristic time τ_f). For large amplitude angular jumps, the loss of angular correlation is a function of the size of the angular jump. If the probability of making a jump is spatially isotropic, this results in the so called Ivanov jump model[87] and a convenient analytical expression for τ_r,

$$\frac{1}{\tau_r} = \frac{1}{\tau_{ex}} \left[1 - \frac{1}{5} \frac{\sin\left(\frac{5\Delta\theta}{2}\right)}{\sin\left(\frac{\Delta\theta}{2}\right)} \right] + \frac{1}{\tau_f} \tag{2}$$

The three quantities on the right hand side of equation 2 are all directly calculated from the simulation for waters belonging to the hydration shell of each sugar oxygen. $\Delta\theta$ is the difference between the average θ before and after the jump event and is calculated from the data shown in Figures 6(a) and 7(a).[88] The resulting values for each water subpopulation are tabulated in the supporting information. The characteristic frame rotation time (τ_f) can be directly quantified by calculating the rotational anisotropy using Equation 1 between large amplitude angular jumps. Characteristic times, resulting from exponential fits to these results, are summarized in Table 3 (see Supporting Information for plots of the frame rotation component of the rotational anisotropy and time constants of frame relaxation for all water subpopulations).[89] Finally, the characteristic time of jump occurence (τ_{ex}) is directly obtained from each trajectory as the inverse of the jump rate constant (k_{ex}) calculated using the Bennet-Chandler approach:[90] as the forward flux across a surface located between stable reactant and product states. Details of this calculation are discussed at length in the supporting information. The resulting characteristic hydrogen bond exchange times for subpopulations of waters initially within 3.5 Å of each sugar oxygen and hydrogen bonded to other waters or to sugar oxygens calculated in this manner are summarized in Table 4. Values of τ_{ex} for all water subpopulations are tabulated in the supporting information.

Given $\Delta\theta$, τ_{ex} and τ_f we solve equation 2 and calculate the rotational anisotropy. If the τ_r calculated in this manner and that directly taken from the simulation agree, this suggests that the assumption of an isotropic jump probability is justified and that rotational anisotropy is well described as the sum of the large amplitude angular jump and an independent diffusive process.

Table 3: Frame decay time constants (τ_f) obtained for different SPC/E water subpopulations from fits of single exponentials to data shown in the Supporting Information[a].

	Population	Trehalose	Kojibiose
Linking Oxygen	W→W	18 (1)	11.0 (0.8)
	W→S	28 (2)	19 (1)
Other Oxygens	W→W	8.5 (1.3)	7.6 (1.1)
	W→S	19.4 (3)	16.8 (3.2)

a For SPC/E water in the bulk the characteristic time of frame rotation is 5.2 ± 0.5 ps. The values in parentheses are the the standard deviation of the average time constant for all oxygens except the linking one and the statistical uncertainty associated with the time constant for the linking oxygen. This uncertainty is estimated by fitting exponential curves to different subsets of the data and reporting the largest difference between the time constants.

Table 4: Characteristic time of hydrogen bond exchange, τ_{ex}, for the indicated SPC/E water subpopulation[a].

	Population	Trehalose	Kojibiose
Linking Oxygen	W→W	7.9 (0.5)	6.0 (0.5)
	W→S	11.4 (0.5)	4.4 (0.5)
Other Oxygens	W→W	5.0 (0.5)	4.6 (0.3)
	W→S	5.7 (1.7)	4.6 (1.1)

a For SPC/E water in the bulk, using the same protocol, the characteristic τ_{ex} is 4.1 ± 0.5 ps. The values in parentheses are the standard deviation of the average τ_{ex} for all oxygens except the linking one, or the statistical uncertainty associated to τ_{ex} of the linking oxygen. The latter is estimated by calculating τ_{ex} using subsets of different length of the simulation trajectory and taking the largest difference between the obtained τ_{ex} for each water population as the uncertainty.

As demonstrated by others (although they calculated τ_{ex} in a different manner[28]) we find this is clearly the case for water in the bulk: the anisotropy decay time calculated taking as input the frame decay time $\tau_f = 5.2$ ps, the jump time $\tau_{ex} = 4.1$ ps and the jump angle $\Delta\theta = 66^\circ$ is $\tau_{r,calc} = 2.4$ ps. while the directly measured anisotropy decay time for water in the bulk from our simulations is $\tau_{r,meas} = 2.3 \pm 0.5$ ps. Results of this approach for water near sugars are shown in Figure 8. Within the numerical accuracy agreement is also clearly quantitative for all four data sets. Comparison

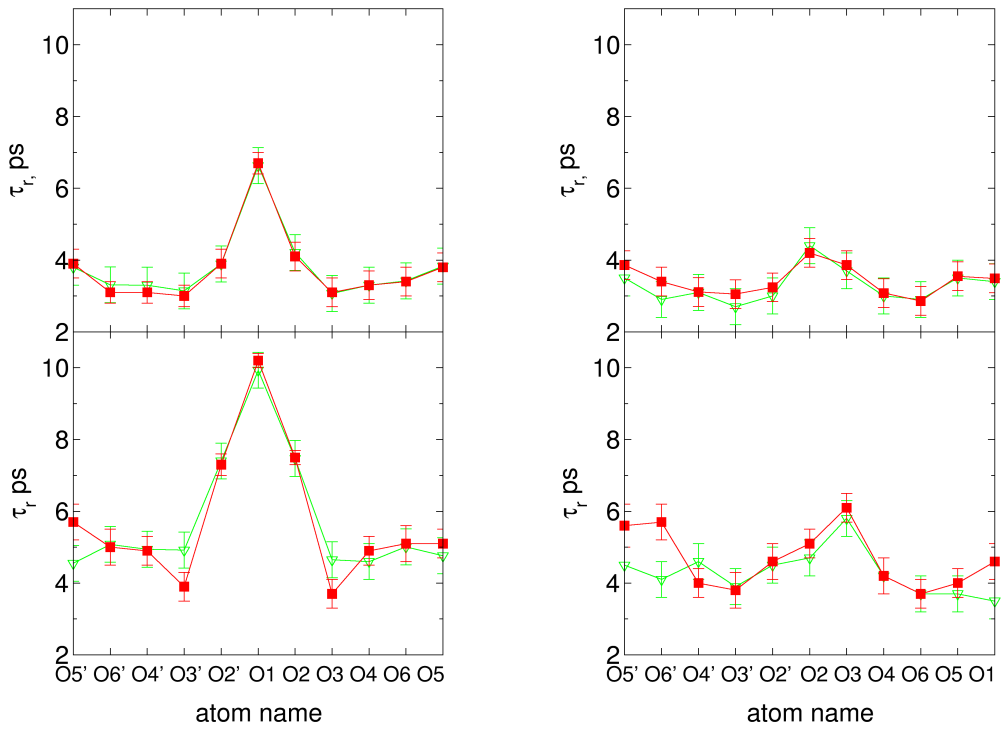

(a) (b)

Figure 8: Rotational anisotropies for different water subpopulations near (a) Trehalose and (b) Kojibiose. Filled (red) points are directly calculated rotational anisotropies of water initially within 3.5 Å of the indicated sugar oxygens. Empty (green) points are the result of solving equation 2. The lines are guides to the eye. The top two graphs contain results for waters that are hydrogen bonded to other waters and initially within 3.5 Å of the indicated sugar oxygen. The bottom two graphs contain results for waters hydrogen bonded to sugar oxygens and initially within 3.5 Å of the indicated sugar oxygen. Statistical uncertainty (indicated by the error bars) was calculated by adding in quadrature the uncertainty of the variables in equation 2 for the green points, or by fitting different subsets of the anisotropy decay curves shown in Figure 3 to single exponentials and taking the largest difference in the obtained time constants for each water subpopulation for the red points.

of Table 2, Table 3 and Table 4 clarifies that, while slowdown in frame rotation is notable as a water molecule moves from bulk to a sugar solvation shell, the hydrogen bond exchange rate is also significantly slowed. Because the exchange term (first term on the rhs of equation 2) is large relative to the frame rotation term, to quantitatively understand water rotational anisotropy in the sugar hydration shell it is important to first gain further insight into the slowdown in hydrogen bond exchange rate.

To do so, it is useful to adopt a thermodynamic formalism: to describe hydrogen bond exchange as a chemical reaction. Following prior work we employ a transition state theory approach to describe the free energy of this process.[26–28,41–43] Within this formalism the rate of hydrogen bond exchange (k_{ex}) can be written (where $\Delta G^{\dagger} = G^{\dagger} - G^{R}$: the free energy difference between the transition and reactant states, κ is the transmission coefficient, A is the prefactor and k_B is the Boltzmann constant),

$$k_{ex} = \frac{1}{\tau_{ex}} = \kappa A \exp\left[-\frac{\Delta G^{\dagger}}{k_B T}\right] \tag{3}$$

Employing the same definition of the transition, reactant and product states as described above for the calculation of τ_{ex} we directly extract from our simulations κ and $\Delta G^{\dagger}$ (see the Supporting Information for more details of this calculation).

Within this analysis we find a $\Delta G^{\dagger}$ of 2.7 ± 0.1 kcal/mol and a κ of 0.52 for water in the bulk. Our value for κ for SPC/E water in the bulk is comparable to that previously reported ($\kappa = 0.53$)[28] for this water model (SPC/E) calculated in a different manner. However our value of $\Delta G^{\dagger}$ is 0.7 kcal/mol higher than this previous study.[28] We expect the explanation for this discrepancy lies in the fact that $\Delta G^{\dagger}$ in this previous effort was calculated from the averaged reaction path while our approach (see discussion in Supporting Information) avoids such averaging.

The calculated $\Delta G^{\dagger}$ for each water subpopulation around the sugars is shown in Figure 9 ($\Delta G^{\dagger}$ and κ for each water subpopulation are also tabulated in the Supporting Information). We note that the values of the prefactor A in equation 3 are directly obtained from $\Delta G^{\dagger}$, κ and k_{ex} and were found to be similar for all water populations considered ($A = 41 \pm 10\%$) as expected. Values of κ range from 0.49 to 0.77. Because κ and A are similar between water subpopulations, and because τ_r is

predominantly a function of τ_{ex} and $\Delta\theta$, we expect differences in $\Delta G^{\dagger}$ to correlate with differences in τ_r. Qualitatively, inspection of Figure 9 confirms this expectation: in general both τ_r and $\Delta G^{\dagger}$ increase as water moves from bulk, to water→water interactions near either sugar to water→sugar interactions. Restricting ourselves to just the water→water hydrogen bonds, comparison of Fig-

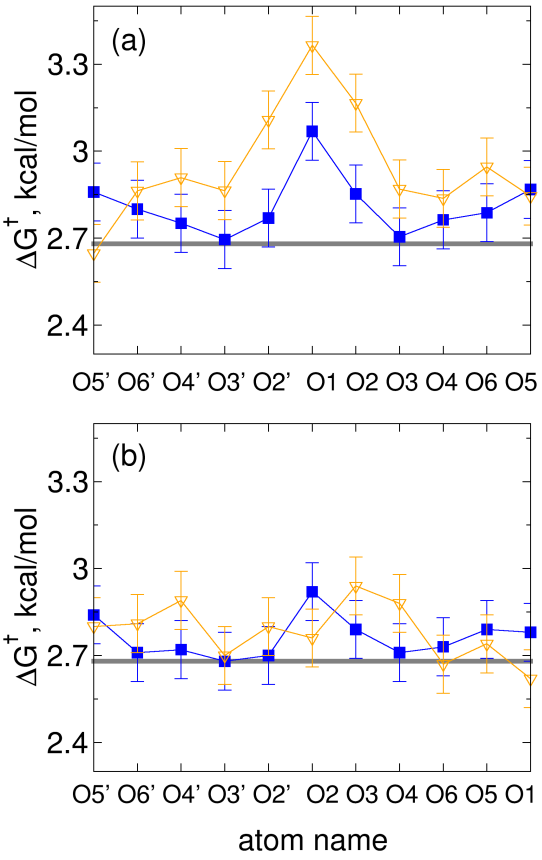

Figure 9: Calculated free energy of hydrogen bond exchange ($\Delta G^{\dagger}$) for (a) Trehalose and (b) Kojibiose subpopulations of water initially within 3.5 Å of the indicated sugar oxygens. Water→water hydrogen bonds are shown in filled symbols (blue), water→sugar hydrogen bonds in empty symbols (yellow). Lines are guides to the eye. Statistical uncertainty (indicated by the error bars) was estimated by calculating the free energies using subsets of different length of the simulation trajectory and taking the largest difference between the obtained free energies as the uncertainty. The horizontal grey line indicates $\Delta G^{\dagger}$ for SPC/E water in the bulk.

ure 8 and Figure 9 makes clear that trends in the directly calculated rotational anisotropies between different water subpopulations correlate with changes in $\Delta G^{\dagger}$. For example, for Trehalose an increase in $\Delta G^{\dagger}$ for water near O2′, O1 and O2 correlates with a rotational slowdown of water near

these atoms, while for Kojibiose a more subtle slowdown of water near O5′, O2 and O3 also seems to correlate with an increase in $\Delta G^{\dagger}$ for water near these atoms.

For water→sugar hydrogen bonds the correlation between $\Delta G^{\dagger}$ and rotational slowdown is less obvious. Clearly for Trehalose the slowest rotating subpopulations of water, those near O2′, O1 and O2, also have the largest $\Delta G^{\dagger}$. On the other hand water near O5′ has a smaller $\Delta G^{\dagger}$ than water near all other sugar oxygens, yet τ_r (see Figure 8) of water near this oxygen is similar to that of water near, for example, O6, O6′, O4 and O4′. Inspection of $\Delta\theta$ for each of these populations (tabulated in the Supporting Information) clarifies that water near O5′ has a τ_r comparable to its neighbors – despite the lower $\Delta G^{\dagger}$ – because its $\Delta\theta$ is 6-15° less. Essentially each angular jump made by water near O5′ leads to less loss of rotational correlation than that in water near other Trehalose oxygens.

For water→sugar hydrogen bonds near Kojibiose both the changes in rotational anisotropy decay and in $\Delta G^{\dagger}$ are smaller and less correlated between water subpopulations than for Trehalose. Here, large calculated $\Delta G^{\dagger}$ correlate with slow rotational dynamics for water near O3, but not near O4 or O4′ while low values of $\Delta G^{\dagger}$ for water near O5′ and O6′ do not correlate with fast rotational anisotropy decay. Comparison of Figure 8, Figure 9 and values of $\Delta\theta$ tabulated in the Supporting Information makes clear that some of these differences can be explained by differences in $\Delta\theta$: waters near O5′, O5 and O2 have small $\Delta\theta$s relative to other water subpopulations, thus their τ_r are somewhat larger than would be predicted based on their $\Delta G^{\dagger}$. In contrast, the lack of correlation between $\Delta G^{\dagger}$ and τ_r for O4 or O4′ arises from the faster frame decay for water around these two sugar oxygens. The opposite effect is observed around O1: the observed τ_r around this atom is comparable to that seen around O4 while its frame decay is slower than O1.

While the analysis presented above demonstrates that water within the hydration shell of Kojibiose and Trehalose undergoes significant changes in τ_{ex} due to changes in $\Delta G^{\dagger}$ it does little to provide a molecular level picture. To do this we need to decompose $\Delta G^{\dagger}$ into its components. Following standard thermodynamic considerations $\Delta G^{\dagger}$ is composed of entropic and enthalpic

contributions,

$$\tau_{ex} \propto \exp\left[\frac{\Delta G^{\dagger}}{k_B T}\right] = \exp\left[\frac{-\Delta S^{\dagger}}{k_B} + \frac{\Delta H^{\dagger}}{k_B T}\right] \tag{4}$$

We can substantially simplify equation 4 if, following prior authors, we approximate the entropic contribution to $\Delta G^{\dagger}$ as $\Delta S^{\dagger} \approx k_B \ln(\Omega^{\dagger}/\Omega^{R})$, where $\Omega^{\dagger}$ is the volume of the transition state and Ω^{R} that of the reactant.[41] Examination of the averaged geometric parameters near jump events, i.e. the data in Figure 6 and Figure 7, suggests, particularly for water→water interactions, it may be reasonable to assume that changes in $\Delta H^{\dagger}$ and Ω^{R} are small moving from water in the bulk to sugar hydration water and from subpopulation to subpopulation around each disaccharide,

$$\tau_{ex} \propto \frac{\Omega^{R}}{\Omega^{\dagger}} \exp\left(\frac{\Delta H^{\dagger}}{k_B T}\right) \propto \frac{1}{\Omega^{\dagger}} \tag{5}$$

Armed with these assumptions, equation 5 suggests that, given the τ_{ex} and transition state volume for SPC/E water in bulk as well as the transition state volume for water in a sugar hydration shell we can calculate τ_{ex} for each water subpopulation around each sugar. Because we are interested in *relative* transition state volumes we have calculated, instead of the transition state volume, the fraction of the transition state unavailable (transition state excluded volume: f) due to the presence of a sugar molecule as described by Laage, Hynes and co-workers.[41] Further details of the excluded volume calculation are discussed, and the resulting calculated f values for each water subpopulation tabulated in the supporting information.

Armed with these excluded volumes we can write,

$$\frac{\tau_{ex}^{sugar}}{\tau_{ex}^{bulk}} = \frac{1}{1-f} \tag{6}$$

Given our calculated values of τ_f, $\Delta\theta$ and f for each water subpopulation we can substitute Equation 6 into Equation 2 and test our ability to reproduce the directly calculated rotational anisotropy in the so called Transition State Excluded Volume (TSEV) model. This approach results in, as shown in Figure 10, a quantitative description of τ_r for neither water→water nor water→sugar

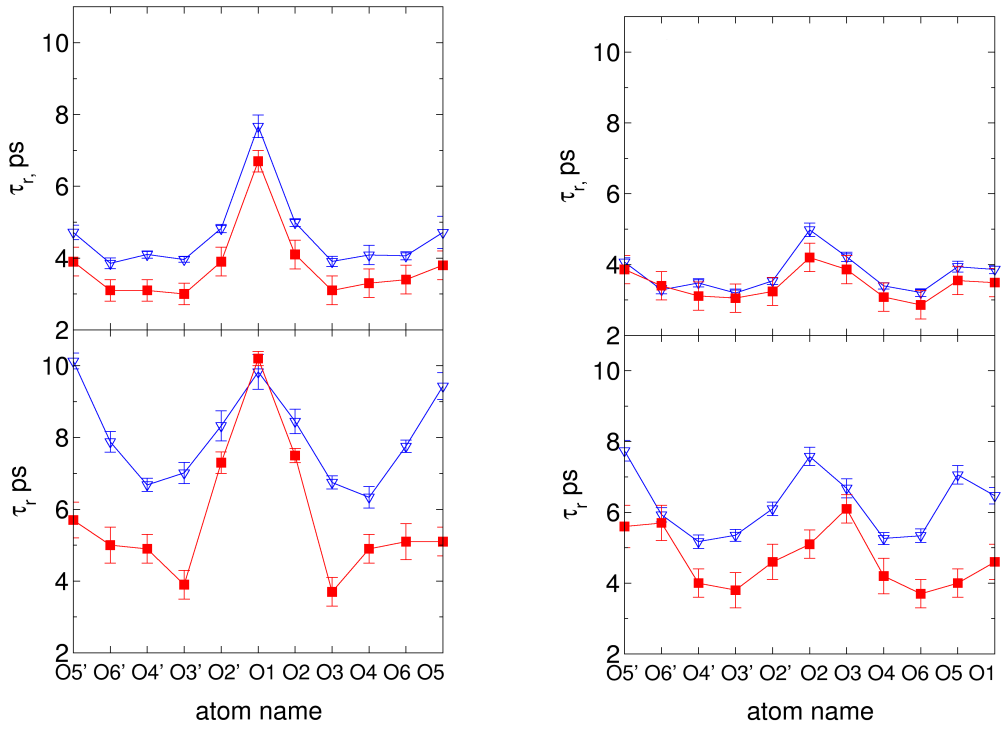

(a) (b)

Figure 10: Comparison of rotational anisotropy decay times (τ_r) calculated with equation 2 and using either the transition state excluded volume approach to obtain τ_{ex} as described in the text (shown in blue) or the directly measured τ_{ex} (shown in red) for column (a) Trehalose or column (b) Kojibiose. Water→water hydrogen bonds for water in the hydration shell of the sugars are shown in the upper panels, water→sugar hydrogen bonds in the lower panels.

interactions. For water→water hydrogen bonds the model overpredicts τ_r by $\approx$ 0.5-1 ps for both Kojibiose and Trehalose but still captures the relative variations in τ_r observed for water near different sugar sites, whereas for water→sugar interactions near either sugar the failure is more dramatic. Here the model overpredicts τ_r by as much as 4 ps and fails to capture the relative magnitudes of τ_r of water near the different sugar oxygens.

Previous work examining water dynamics near amphiphilic amino acids has pointed out that the TSEV model would be expected to fail (and in fact does) for individual OH groups that donate hydrogen bonds to acceptors that are either stronger or weaker than water in the bulk:[43] in systems where either H^R or S^R might differ from water in the bulk. With these results in mind, it is perhaps unsurprising that the TSEV model fails for water→sugar interactions. However, this model has been shown to be sufficient to describe the slowdown of water dynamics in the hydration layer of small hydrophobic solutes[41] and for water→water interactions near amino acids:[43] systems in which water OH groups are close, but not hydrogen bonded to a solute. For this reason the evident failure of the TSEV model to quantitatively describe slowdown in water→water interactions in the sugar hydration shell is more suprising.

Given that for these types of interactions the TSEV model overpredicts the measured anisotropies by only $\approx$ 0.5-1 ps, it is reasonable to ask if this failure is an artifact introduced by the particular way the transition state excluded volume fractions are calculated. We emphasize that this is not the case because (as explained in detail in the Supporting Information), our manner of calculating the excluded volume produces a lower bound for the effect of excluded volume on τ_r: alternative methods of calculating the TSEV would likely lead to a larger difference between modeled and directly calculated τ_r than that shown in Figure 10. The observed failure of the TSEV model for the water→water subpopulation near sugars is thus in apparent conflict with the conclusions of Sterpone et al. for water→water interactions near amino acids.[43] As noted above, in that study, the authors concluded that the rotational slowdown of water→water subpopulations near hydrophobic amino acids was correctly predicted by the TSEV model. Close examination of their reported results, however, indicates that also in that case the TSEV model in general overestimated the

slowdown experienced by water by ≈ 0.5 ps.

A quantitative decomposition of the reasons for this overprediction of τ_r for all water subpopulations near sugars is beyond the scope of this paper, but we can point to several qualitative factors that should perturb the excluded volume scaled results in the sense we observe. As mentioned above, $\Delta G^{\dagger} = G^{\dagger} - G^{R}$. The scaling results shown in Figure 10 assume that all changes in $\Delta G^{\dagger}$ as one moves from SPC/E water in the bulk, to water→water interactions within the sugar solvation shell to water→sugar hydrogen bonds are the result of changes in the entropy of the transition state, i.e. changes in $S^{\dagger}$. The model also assumes that the transition state geometry is the same for water in the bulk and water near solutes, with changes in $S^{\dagger}$ arising solely from the steric impediment to transition state configurations brought by the presence of the solute. If, following prior work,[28] we assume the contribution of the transition state for hydrogen bond exchange can be effectively described by a two dimensional reaction coordinate – where one dimension is θ and the other the difference of the two relevant distances, i.e. Δd =$\mathrm{O}_d \cdots \mathrm{O}_o$ - $\mathrm{O}_d \cdots \mathrm{O}_n$ – we can evaluate these assumptions about the nature of the transition state by constructing 2 dimensional histograms of transition state configurations for all successful hydrogen bond exchanges. Extracting contours of constant probability from each histogram describing water→water and water→sugar interactions near a particular sugar oxygen and comparing then with a contour of the same probability in water in bulk allows a description of how transition state configurations change as water moves closer and then interacts with an oxygen on either sugar.

Results of this analysis are shown in Figure 11 and result in several immediate conclusions. Firstly, it is clear that the assumption that the transition state geometry is similar for water near sugars and for water in the bulk does not hold: the transition state of water→water and water→sugar hydrogen bonds is significantly broader than those in bulk. While this broadening is more marked for water→sugar subpopulations, it is already clearly present for water→water interactions as well. Secondly, the transition state broadening is largely independent of the chemical character of nearby sugar functional groups: similar trends are observed for transition states involving water near sugar oxygens with very different polarities. Thirdly, the broadening is not symmetric; instead, we ob-

serve an extension of the transition state towards negative values of Δd and θ. These negative values indicate that during hydrogen bond exchange for water molecules in the sugar hydration shell the new acceptor is further from and the old acceptor closer to the donor than for the same process in bulk. This has two implications. First, the true transition state excluded volume is smaller than that calculated above and used to predict the values of τ_r shown in Figure 10. Second, the average *enthalpy* of the transition state associated with hydrogen bond exchange of water near sugars is more negative than for water in the bulk because configurations in which the donor and old acceptor are closer together are still abundant in the transition state; in water in the bulk these enthalpically favorable transition state configurations are largely absent. Both these effects lead to a lower $G^{\dagger}$, and hence smaller τ_r, than that estimated using the TSEV model.

Inspection of Figure 10 shows that for water→water interactions the TSEV predicts relative trends in τ_r both between different water subpopulations on a single sugar and between sugars but systematically over-predicts τ_r by $\approx$ 0.5-1 ps for all water subpopulations. As discussed above, transition state broadening, as one moves from bulk to water→water, to water→sugar subpopulations is also relatively insensitive to sugar type and water subpopulation and will result in a decrease in $\Delta G^{\dagger}$ (increase in τ_r). Thus the systematic overestimation of τ_r for water→water hydrogen bonds seems most easily understood as the result of this effect.

As described above, the TSEV model was developed to explain the slowdown in water rotation observed around nominally hydrophobic solutes.[41] Put in thermodynamic terms the premise of this model is that the slowdown in rotation can be quantitatively explained by an increase in $\Delta G^{\dagger}$ that is due exclusively to an decrease in $S^{\dagger}$. If the change in $\Delta G^{\dagger}$ as a water molecule moves from bulk to a hydrophobic hydration shell contains no enthalpic contribution one would expect that the activation energy, as inferred from an Arrhenius plot of rotation rate as a function of temperature, should be the same for water molecules in the hydrophobic hydration shell as in bulk. In a recent study by Tielrooij and coworkers water rotation dynamics were measured around tetramethyl urea (TMU) as a function of temperature using both ultrafast time resolved IR pump / probe spectroscopy and dielectric relaxation.[40] The combination of these two techniques allowed them to conclude that

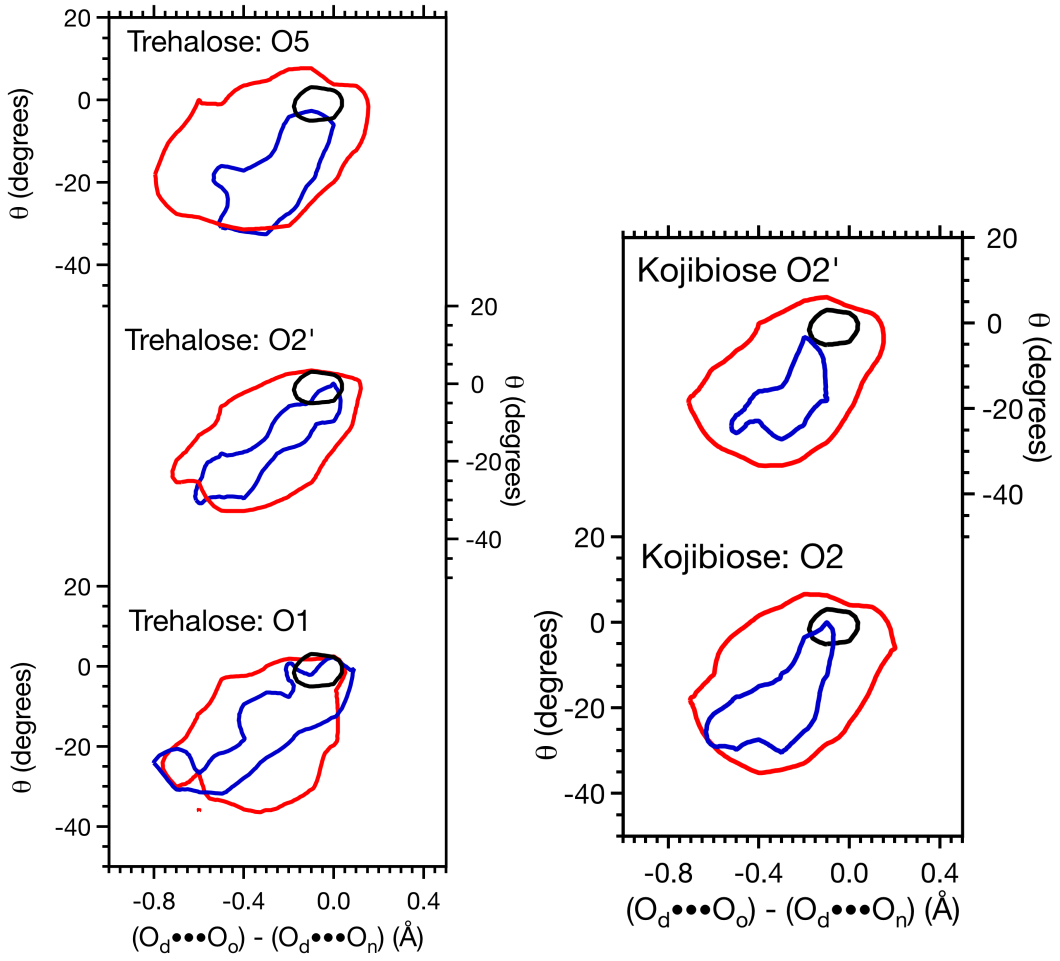

Figure 11: Comparison of 0.012 probability density contours describing transition state geometries during successful hydrogen bond exchange events (water rotations), in water in the bulk (black) and for water→water (blue) and water→sugar (red) interactions within 3.5 Å of the indicated sugar oxygens. In every case the populated transition state configurations broaden on moving from bulk to water→water interactions near a sugar to water→sugar interactions.

water within the methyl hydration shell of TMU has significantly different activation energy for rotation than does water in bulk thus suggesting the energetics of water rotation in the hydrophobic hydration shell differ from that in water in the bulk due to an enthalpic contribution. The water→water interactions in the Kojibiose and Trehalose hydration shell are qualitatively similar to those in the methyl hydration shell of TMU: both involve hydrogen bonds that are approximately tangential to the underlying solute. In analogy to the sugar hydration shell our results suggest that water rotation in the hydration shell of TMU likely undergoes transition state broadening. Because such broadening implies an enthalpic contribution to the increase in $\Delta G^{\dagger}$ it would provide a convenient mechanism to reconcile the experimental and previous simulation results and seems likely to be a general feature of hydrophobic hydration.

For water→sugar populations Figure 10 shows that the TSEV model largely fails to predict relative trends in τ_r and that the difference between the modeled and directly calculated value of τ_r varies strongly as a function of water subpopulation and sugar type. Because sugar induced transition state broadening is relatively insensitive to water subpopulation, we must look for a different explanation. We ask whether solute induced changes in G^R may be implicated in the observed increases in τ_r. As discussed above, for waters donating hydrogen bonds to hydrophilic amino acids, Sterpone et al. have demonstrated that slowdown due to changes in G^R occurs. They did this by performing a potential of mean force calculation for the increase in $O_d \cdots O_o$ distance that occurs before the jump, i.e. by calculating the contribution of this process to the total $\Delta G^{\dagger}$. They find that this free energy of stretching an existing hydrogen bond is, in general, larger for water→amino acid hydrogen bonds than water in the bulk and that this effect, when combined with the TSEV model, explains the slowdown of waters donating hydrogen bonds to hydrophilic amino acids.

The free energy cost of stretching any hydrogen bond is composed of both an enthalpic and entropic component. Because the enthalpic contribution to the free energy of hydrogen bond stretching is largely determined by pair wise interactions between H-bond donor and acceptor, within the context of our simulation we can gain insight into whether the enthalpy of hydrogen

bond stretching is likely to explain differences in the dynamics of water→sugar subpopulations by comparing the partial charges and van der Waals parameters on oxygen atoms. In Kojibiose, O3, O4, O6, O2′, O3′, O4′ and O6′ are all similar, with O1 having slightly lower charge while the ring oxygens, O5′ and O5, and the linking oxygen, O2, both have substantially less charge. Similarly, for Trehalose, O2, O3, O4, O6, O2′, O3′, O4′ and O6′ all have similar partial charges and VdW parameters while O5 and O5′ are less charged and O1 (the linking oxygen) still less. These trends suggest, then, that the G^R of waters involved in hydrogen bonds to O5 or O5′ may be different than the G^R of those waters donating hydrogen bonds to any of the hydroxyl oxygens (recall that the linking oxygens, O2 in Kojibiose and O1 in Trehalose accept virtually no hydrogen bonds from water) due to changes in enthalpy of the reactant state: H^R.

We can estimate whether G^R is likely to differ between water subpopulations by calculating the one dimensional oxygen-oxygen radial distribution function (rdf) around each sugar oxygen.[91] The volume occupied by the solute is not excluded in this calculation so this rdf reflects also free energy changes (relative to the ideal gas) arising from the reduction in the number of available configurations as water comes closer to the sugar. The results of this analysis are shown in Figure 12. Clearly the rdf around O5 and O5′ (note that because of symmetry these two oxygens are equivalent in Trehalose but not Kojibiose) differs from water in the bulk. Qualitatively these hydrogen bonds to the less polar ring oxygens appear to be looser suggesting that H^R is less negative and hence $\Delta G^\dagger$ is reduced for these water subpopulations. Not accounting for this effect (as in the TSEV model) should lead, as we observe, to an overestimation of τ_r for these water types.

While likely important in describing the dynamics of water near the ring oxygens, an enthalpic contribution to G^R cannot explain the anomalous dynamics observed in water near the linking oxygens (O1 in Trehalose, O2 in Kojibiose) as in both cases there are virtually no hydrogen bonds donated by water to these oxygens. Similarly, this effect cannot explain differences in dynamics observed in water near the various hydroxyl oxygens (e.g. O3 and O2 in Trehalose) as these oxygens both have the same force field parameters. We thus expect that changes (relative to bulk) in the entropy S^R of the reactant state should also occur for these water→sugar subpopulations.

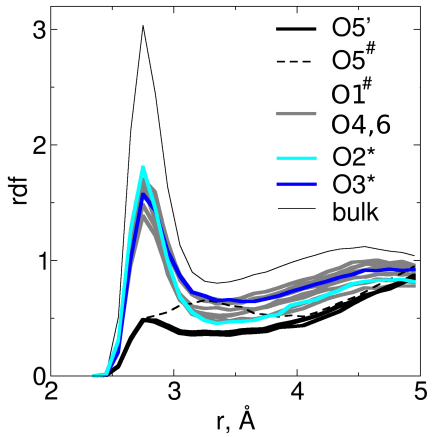

Figure 12: Oxygen/oxygen radial distribution function around each sugar oxygen and in water in bulk (obtained using the SPC/E water model). The superscript # denotes a subpopulation of water near the indicated atom in Kojibiose, the superscript * indicates the same in Trehalose. Absence of either superscript indicates equivalent subpopulations in both sugars. The rdf for water in the bulk (thin black line) is qualitatively similar to that of water near all hydroxyl oxygens in both sugars (grey band). Clearly the rdf of water near O5 and O5′ in Trehalose and O5′ in Kojibiose (thick black line) as well as that near O5 in Kojibiose are qualitatively different and consistent with a more weakly hydrogen bonded subpopulation of water molecules.

To investigate this possibility we again look to the rdf curves shown in Figure 12. Examination of the rdf around O3 and O2 in trehalose between $r = 2.8$ Å (reactant state) and $r = 3-4$ Å (transition state) confirms that the two curves do not overlap and indicates that differences in $\Delta G^{\dagger}$ between these two sites noted previously in Figure 9 arise not only from changes in $G^{\dagger}$ but also from changes in G^{R}. Because O2 and O3 have the same force field parameters, differences in G^{R} for water→sugar interactions necessarily arise due to differences in the number of available configurations of the reactant state. We can estimate the contribution of the elongation of the original water→sugar hydrogen bond to $\Delta G^{\dagger}$ for O2 and O3 by calculating $-k_B T \ln\left(\frac{G(r=3.5)}{G(r=2.8)}\right)$. We find that this contribution is ≈ 0.3 kcal/mol larger for water near O2 than water near O3, in quantitative agreement with the difference in $\Delta G^{\dagger}$ between these two water populations shown in Figure 9.

To this point, none of the characteristics of the water→sugar interactions discussed above explain why the TSEV model correctly predicts the slowdown of water within 3.5 Å of the linking

oxygen of Trehalose (O1) and hydrogen bonded to sugar oxygens. This prediction is, on its face, puzzling. As we have discussed above, transition state broadening effects are not remarkably different for this water subpopulation than for a variety of other water→sugar subpopulations. Similarly, virtually all of the water in this subpopulation donates a hydrogen bond to one of the neighboring sugar oxygens (principally O2 and O2′) thus suggesting H^R and S^R are unlikely to be dramatically different than other waters hydrogen bonded to these acceptors. However, in the discussion offered above, we have not yet considered the work necessary (i.e. the contribution to the free energy barrier to hydrogen bond exchange) to move the new acceptor to the transition state. If, for a given aqueous system, this work is larger than that in water in bulk, the TSEV prediction would be closer to the real value. Sterpone et al. have previously proposed that this contribution to rotational slowdown is likely to become important for water in nanoconfinement.[43] It appears,then, that for the linking oxygen of trehalose the TSEV prediction is correct because the overprediction of the TSEV model fortuitously compensates the lack of accounting for the extra work necessary to bring the new acceptor to the transition state at that location.

It is important to emphasize that *confinement* in this sense is related, but not equivalent to the transition state excluded volume. In a molecular level picture the former effect is the work necessary to bring the new acceptor from the hydrogen bond donor's second hydration shell to the transition state, while the transition state excluded volume quantifies the decrease in the number of paths over which this transition might occur. Thus, while changes in the transition state excluded volume imply changes in the free energy barrier to bring the new acceptor to the transition state, the converse is not true. While definitive demonstration of this new acceptor approach effect would require a pmf calculation beyond the scope of this study it is worth emphasizing that other observables are consistent with this effect.

As discussed in detail above, the rotation of individual water molecules requires two translation steps (the translation of the old acceptor away from and the new acceptor toward the donor). As a result, environments in which translation is dramatically slowed are expected to have slowed rotation. As mentioned above, calculation of the mean square displacement of all water subpop-

ulations in the hydration shell of each sugar shows that water translation is markedly slower near the linking oxygen of Trehalose than in all other water subpopulations. To gain some insight into why translation slows, additional metrics are required.

A prior computational study by Lee et al. of water within 5 Å of Glucose, Trehalose and Sucrose over $0-30^{\circ}$C showed that water within the hydration shell of these molecules experiences a pronounced decoupling of rotation and translation (where rotation is defined by a rotational correlation function identical to our equation 1 but without the factor of $\frac{2}{5}$ and translation is defined by the diffusion constant). This decoupling, although caused by the presence of the solute, is analogous to that seen in supercooled liquids: extensive prior work describing the structure of water in bulk as it is cooled below 0°C also has demonstrated that this regime is characterized by water density fluctuations of increasing amplitude and life time.[92,93] As mentioned previously, water near either sugar shows density fluctuations of dramatically higher amplitude than those in bulk (see Table 1). To demonstrate that these larger density fluctuations were also longer lived, we calculated a density autocorrelation function (in which N is hydration number within 3.5 Å of each sugar oxygen or, for water in bulk, within that distance of a given water molecule, and δ the Kroenecker delta),

$$C(\tau) = \langle \delta \left(N(\tau) - N(0) \right) \rangle \tag{7}$$

The above average is over all time origins. The decay curves resulting from this calculation are shown in the supporting information. The density autocorrelation decays significantly more slowly for water near the linking oxygen of Trehalose than water near all other sugar oxygens and clearly water near a sugar has longer lived density fluctuations than water in the bulk. Time constants for each of the decay curves are shown in Table 5. We are thus in an environment near the Trehalose linking oxygen in which translation and rotation are dramatically slowed and density fluctuations are both much larger and longer lived relative to water in bulk and all other subpopulations of water around either sugar.

In principle these characteristics of the subpopulation of water near the Trehalose linking oxygen – dramatically slowed translation, relatively large and long lived density fluctuations – might

Table 5: Characteristic time (in ps) of the decay of the density autocorrelation function extracted from a single exponential fit, with different end levels, to the data shown in the supporting information.

	Trehalose	**Kojibiose**
Linking Oxygen	3.8	1.5
O5, O5′	1.2	1.2
Other Oxygens	0.8	0.7
Bulk Water	0.4	

be expected to influence both OH groups that are hydrogen bonded to sugar oxygens and those hydrogen bonded to other water molecules. Inspection of Figure 10 makes clear that this is untrue. Rotational slowdown of water near the Trehalose linking oxygens but hydrogen bonded to other water molecules (water→water interactions), can be fairly well described by accounting for transition state excluded volume and broadening effects. Absent detailed description, perhaps through transition path sampling, of the transition of the new acceptor from the second to the first hydration shell of the donating OH we cannot explain this difference. However we note, in agreement with the suggestion of Sterpone et al., that the free energy barrier to this translation of the new acceptor is likely to be far larger the greater the confinement and that it seems plausible that water donating a hydrogen bond to a sugar oxygen in this subpopulation is more confined than water→water.

We have, to this point, focussed on discussion of the change in hydrogen bond exchange rate (i.e. τ_{ex}) as water moves from bulk into the sugar hydration shell. As shown in Table 3 and in more detail in the supporting information, however, frame rotation (diffusive rotation of water molecules between jump events) also slows in the sugar hydration shell. Reference to Table 3 highlights that frame rotation always slows more for water→sugar interaction than for water→water both of which are significantly slower than water in the bulk . The former effect, that water→sugar interactions have a slower frame rotation than water→water, can be rationalized by recognizing that frame rotation requires the rotation of both the hydrogen bond donor and the acceptor relative to an external reference frame. Because, in the case of the water→sugar interactions this acceptor is far more massive and slower rotating we expect, as we indeed observe, that such rotation should

be slowed. The slowdown of frame rotation in water→water interactions in the sugar hydration shell, relative to water in the bulk, can be rationalized similarly. In our description of water→water populations we require only that an individual water OH be within 3.5 Å of the indicated sugar oxygen and donate a hydrogen bond to another water molecule. We do not impose any restrictions on the other OH in the hydrogen bond donating water molecule. If this OH is hydrogen bonded to a sugar oxygen we would expect, for reasons similar to that described above, that this hydrogen bonded pair should have a frame rotation rate somewhat decreased relative to water in the bulk.

Aside from the general trends described above, inspection of Table 3 highlights that for each type of interaction, i.e. water→water or water→sugar, water near the Trehalose linking oxygen has a dramatically slower frame rotation than all other water types. While the molecular mechanism of frame rotation is not well understood one might expect that, by analogy to translational diffusion in bulk, individual steps are driven by density fluctuations. Since, as discussed above, such fluctuations are markedly slower in this water subpopulation it is perhaps unsurprising that frame rotation is here also significantly slowed.

Summary and Conclusions

Our results highlight several points that are of relevance in understanding the thermodynamics and structural dynamics of water around large biomolecules. Firstly, as previously demonstrated for several proteins, the differing relative hydrophobicities between, for example, water near the linking oxygen of Trehalose and Kojibiose highlight that local hydrophobicity is context dependent: multiple instances of a particular functional group, e.g. an amino acid in a large protein, can have drastically different hydrophobicities at different places in a single macromolecule. Intriguingly, the metric of local hydrophobicity we employ, time averaged density fluctuations, correlates strongly with local water structural dynamics: water structural dynamics surrounding large biomolecules are also likely strongly context dependent.

To understand the correlation between local hydrophobicity and water structural dynamics we

examined in detail the mechanism of hydrogen bond exchange in all subpopulations of water around each sugar. Previous studies of the dynamics of water around sugars and proteins (featuring polar, but not charged, side chains) have emphasized that the effect of the solute on neighboring water molecules goes to zero, both with respect to translation and rotation, as one reaches 5-6 Å from the solute. This relatively short range effect on dynamics is here clearly illustrated to be the result of how the solute affects the mechanism of hydrogen bond breaking: within the first sugar solvation shell, for OH groups not hydrogen bonded to the solute, we find that rotational dynamics can be quantitatively explained by a position specific transition state excluded volume effect and a relatively nonspecific broadening of the transition state. Both effects, the former explicitly, are strongly a function of local molecular topology and, as such, should go to zero within, perhaps, one additional water layer. In general terms, these water→water interactions paint a picture of altered local hydrogen bonding around polar solutes being lost over short distances. Various physiologically important molecular functions require the motion of specific domains of large proteins. Often this motion is thought to be induced/amplified by differential solvent coupling within different protein domains.[94–96] One consequence of our observations is that the sort of long range coupling this kind of mechanism likely requires cannot be accomplished with merely polar solute moieties; ionic functional groups on the solute are likely required.[97]

Our observation of transition state broadening for OH groups in the solvation shell of either sugar and donating hydrogen bonds to other waters suggests that similar effects may occur within the solvation shell of all nominally hydrophobic solutes (where such systems are also characterized by OH groups acting as hydrogen bond donors to other waters). Such an effect, if found to exist, would potentially reconcile conflict between current simulation and experimental studies of water rotation in such systems.[41,72]

While our observed correlation of local hydrophobicity and water structural dynamics also applies for water→sugar hydrogen bonds it is evident that rotational slowdown cannot here be explained by a simple model that accounts for transition state excluded volume. In some cases it is clear that at least part of the disagreement is the result of a changing enthalpy of hydrogen bonding.

More intriguingly, however in the majority of water populations this seems unlikely to be the case. In some instances, for example, water near O2 and O3 on Trehalose, approximate metrics suggest that the entropy of the reactant (hydrogen bonded) state changes as a function of position around the sugar. In others, for example water near the linking oxygen of Trehalose, it appears that the work necessary to bring the new hydrogen bond acceptor to the transition state also contributes to $\Delta G^{\dagger}$.

The sorts of effects we observe, namely water dynamics near amphiphilic solutes that are dramatically slower than bulk and also strongly contingent on local solute topology, are likely to be a general feature of all biomolecular hydration. Radical changes in water structure, e.g. the dewetting of a ligand pocket just before docking or a hydrophobic patch just before protein folding, are known to be important for molecular physiology. Understanding the solute/solvent coupling in biomolecules would be substantially simplified if a reductionist approach were appropriate: if, for example, a leucine interacted the same with water regardless of whether it was free in solution or within a large protein. Our analysis suggests that such a reductionist approach is unjustified: that water dynamics within a solute's hydration shell is the delicate result of solute/solvent coupling over a variety of length scales (from individual hydrogen bonds to at least a water molecule's second solvation shell) and that we should therefore not expect to quantitatively understand such processes employing a reductionist approach.

Finally, we note that from the point of view of water dynamics beyond the first solvation shell, there appears to be little special about Trehalose. Indeed the observed slowdown of water is solely a function of topology – an effect, in line with previous work, that should be dissipated by the second water solvation shell. This is an additional piece of evidence that any uniqueness in the cryoprotection ability of Trehalose must be the result of either the manner in which this sugar interacts with membranes or differences in properties of concentrated sugar solutions and have little to do with the manner in which single molecules interact with water.

Acknowledgement

This work is part of the research program of the "Stichting voor Fundamenteel Onderzoek der Materie (FOM)" which is financially supported by the "Nederlandse organisatie voor Wetenschappelijk Onderzoek (NWO)". Further financial support was provided by a Marie Curie Incoming International Fellowship (RKC). We gratefully acknowledge SARA, the Dutch center for high-performance computing, for computational time and Huib Bakker and Daan Frenkel for useful critical reviews on an earlier version of this work. We thank two anonymous reviewers for their excellent work, especially for bringing to our attention calculations done on the transition state geometry of dimers and the overstructuring of the O-O radial distribution function of SPC/E water.

Supporting Information Available

Tabulated values of $\Delta\theta$, τ_r, τ_f, $\Delta G^{\dagger}$, κ, τ_{ex} and f for all water subpopulations around each sugar (for definitions of terms see main text), the coordination of old and new hydrogen bond acceptors near jump events, detailed descriptions of the manner in which τ_{ex}, $\Delta G^{\dagger}$, κ and f were calculated, density fluctuation ($C(\tau)$) curves. This material is available free of charge via the Internet at `http://pubs.acs.org`.

Notes and References

(1) Freites, J.; Tobias, D.; von Heijne, G.; White, S. *Proceedings of the National Academy of Sciences of the United States of America* **2005**, *102*, 15059–15064.

(2) Schmidt, D.; Jiang, Q.-X.; Mackinnon, R. *Nature* **2006**, *444*, 775–779.

(3) Johansson, A. C. V.; Lindahl, E. *Journal of Physical Chemistry B* **2009**, *113*, 245–253.

(4) Krepkiy, D.; Mihailescu, M.; Freites, J. A.; Schow, E. V.; Worcester, D. L.; Gawrisch, K.; Tobias, D. J.; White, S. H.; Swartz, K. J. *Nature* **2009**, *462*, 473–479.

(5) Cherepanov, D. A.; Feniouk, B. A.; Junge, W.; Mulkidjanian, A. Y. *Biophysical Journal* **2003**, *85*, 1307–1316.

(6) Cherepanov, D. A.; Junge, W.; Mulkidjanian, A. Y. *Biophysical Journal* **2004**, *86*, 665–680.

(7) Mulkidjanian, A. Y.; Heberle, J.; Cherepanov, D. A. *Biochimica Et Biophysica Acta-Bioenergetics* **2006**, *1757*, 913–930.

(8) Bakker, H. J. *Chemical Reviews* **2008**, *108*, 1456–1473.

(9) Roberts, S. T.; Ramasesha, K.; Tokmakoff, A. *Accounts in Chemical Research* **2009**, *42*, 1239–1249.

(10) Setny, P.; Wang, Z.; Cheng, L.-T.; Li, B.; McCammon, J. A.; Dzubiella, J. *Physical Review Letters* **2009**, *103*, 187801.

(11) Zhou, R. H.; Huang, X. H.; Margulis, C. J.; Berne, B. J. *Science* **2004**, *305*, 1605–1609.

(12) Liu, P.; Huang, X. H.; Zhou, R. H.; Berne, B. J. *Nature* **2005**, *437*, 159–162.

(13) Zhang, L.; Yang, Y.; Kao, Y.-T.; Wang, L.; Zhong, D. *Journal of the American Chemical Society* **2009**, *131*, 10677–10691.

(14) Giovambattista, N.; Lopez, C. F.; Rossky, P. J.; Debenedetti, P. G. *Proceedings of the National Academy of Sciences of the United States of America* **2008**, *105*, 2274–2279.

(15) Hribar, B.; Southall, N.; Vlachy, V.; Dill, K. *Journal of the American Chemical Society* **2002**, *124*, 12302–12311.

(16) Laage, D.; Hynes, J. T. *Proceeding of the National Academy of Sciences of the United States of America* **2007**, *104*, 11167–11172.

(17) Chandler, D. *Nature* **2005**, *437*, 640–647.

(18) Rajamani, S.; Truskett, T. M.; Garde, S. *Proceedings of the National Academy of Sciences of the United States of America* **2005**, *102*, 9475–9480.

(19) Mittal, J.; Hummer, G. *Proceedings of the National Academy of Sciences of the United States of America* **2008**, *105*, 20130–20135.

(20) Jensen, T. R.; Jensen, M. O.; Reitzel, N.; Balashev, K.; Peters, G. H.; Kjaer, K.; Bjornholm, T. *Physical Review Letters* **2003**, *90*, 086101.

(21) Poynor, A.; Hong, L.; Robinson, I. K.; Granick, S.; Zhang, Z.; Fenter, P. A. *Physical Review Letters* **2006**, *97*, 266101.

(22) Poynor, A.; Hong, L.; Robinson, I. K.; Granick, S.; Fenter, P. A.; Zhang, Z. *Physical Review Letters* **2008**, *101*, 039602.

(23) Godawat, R.; Jamadagni, S. N.; Garde, S. *Proceedings of the National Academy of Sciences of the United States of America* **2009**, *106*, 15119–15124.

(24) Acharya, H.; Vembanur, S.; Jamadagni, S. N.; Garde, S. *Faraday Discussions* **2010**, 1–13.

(25) Patel, A. J.; Varilly, P.; Chandler, D. *Journal of Physical Chemistry B* **2010**, *114*, 1632–1637.

(26) Laage, D.; Hynes, J. T. *Science* **2006**, *311*, 832–835.

(27) Laage, D.; Hynes, J. T. *Chemical Physics Letters* **2006**, *433*, 80–85.

(28) Laage, D.; Hynes, J. T. *Journal of Physical Chemistry B* **2008**, *112*, 14230–14242.

(29) Loparo, J. J.; Roberts, S. T.; Tokmakoff, A. *Journal of Chemical Physics* **2006**, *125*, 194521.

(30) Loparo, J. J.; Roberts, S. T.; Tokmakoff, A. *Journal of Chemical Physics* **2006**, *125*, 194522.

(31) Bakker, H. J.; Rezus, Y. L. A.; Timmer, R. L. A. *Journal of Physical Chemistry A* **2008**, *112*, 11523–11534.

(32) Rezus, Y. L. A.; Bakker, H. J. *Physical Review Letters* **2007**, *99*, 148301.

(33) Qvist, J.; Halle, B. *Journal of the American Chemical Society* **2008**, *130*, 10345–10353.

(34) Rezus, Y. L. A.; Bakker, H. J. *Journal of Physical Chemistry A* **2008**, *112*, 2355–2361.

(35) Bakulin, A. A.; Liang, C.; Jansen, T. L. C.; Wiersma, D. A.; Bakker, H. J.; Pshenichnikov, M. S. *Accounts of Chemical Research* **2009**, *42*, 1229–1238.

(36) Fayer, M. D.; Moilanen, D. E.; Wong, D.; Rosenfeld, D. E.; Fenn, E. E.; Park, S. *Accounts of Chemical Research* **2009**, *42*, 1210–1219.

(37) Heisler, I. A.; Meech, S. R. *Science* **2010**, *327*, 857–860.

(38) Ji, M.; Odelius, M.; Gaffney, K. J. *Science* **2010**, *328*, 1003–1005.

(39) Moilanen, D. E.; Wong, D.; Rosenfeld, D. E.; Fenn, E. E.; Fayer, M. D. *Proceedings of the National Academy of Sciences of the United States of America* **2009**, *106*, 375–380.

(40) Tielrooij, K. J.; Garcia-Araez, N.; Bonn, M.; Bakker, H. J. *Science* **2010**, *328*, 1006–1009.

(41) Laage, D.; Stirnemann, G.; Hynes, J. T. *Journal of Physical Chemistry B* **2009**, *113*, 2428–2435.

(42) Stirnemann, G.; Hynes, J. T.; Laage, D. *Journal of Physical Chemistry B* **2010**, *114*, 3052–3059.

(43) Sterpone, F.; Stirnemann, G.; Hynes, J. T.; Laage, D. *Journal of Physical Chemistry B* **2010**, *114*, 2083–2089.

(44) Crowe, L.; Reid, D.; Crowe, J. *Biophysical Journal* **1996**, *71*, 2087–2093.

(45) Crowe, J.; Crowe, L.; Oliver, A.; Tsvetkova, N.; Wolkers, W.; Tablin, F. *Cryobiology* **2001**, *43*, 89–105.

(46) Crowe, L. *Comparative Biochemistry and Physiology A – Molecular and Integrative Physiology* **2002**, *131*, 505–513.

(47) Sakurai, M.; Furuki, T.; ichi Akao, K.; Tanaka, D.; Nakahara, Y.; Kikawada, T.; Watanabe, M.; Okuda, T. *Proceedings of the National Academy of Sciences of the United States of America* **2008**, *105*, 5093–5098.

(48) Branca, C.; Magazù, S.; Maisano, G.; Migliardo, P.; Tettamanti, E. *Physica B-Condensed Matter* **2000**, *291*, 180–189.

(49) Branca, C.; Magazù, S.; Maisano, G.; Bennington, S.; Fak, B. *Journal of Physical Chemistry B* **2003**, *107*, 1444–1451.

(50) Cheetham, N. W. H.; Dasgupta, P.; Ball, G. E. *Carbohydrate Research* **2003**, *338*, 955–962.

(51) Gaida, L. B.; Dussap, C. G.; Gros, J. B. *Food Chemistry* **2006**, *96*, 387–401.

(52) Magazù, S.; Migliardo, F.; Telling, M. T. F. *European Biophysical Journal* **2007**, *36*, 163–171.

(53) Magazù, S.; Migliardo, F.; Ramirez-Cuesta, A. J. *Biophysical Chemistry* **2007**, *125*, 138–142.

(54) Arikawa, T.; Nagai, M.; Tanaka, K. *Chemical Physics Letters* **2008**, *457*, 12–17.

(55) Gharsallaoui, A.; Roge, B.; Genotelle, J.; Mathlouthi, M. *Food Chemistry* **2008**, *106*, 1443–1453.

(56) Magazu, S.; Migliardo, F.; Telling, M. T. F. *Food Chemistry* **2008**, *106*, 1460–1466.

(57) Heugen, U.; Schwaab, G.; Bruendermann, E.; Heyden, M.; Yu, X.; Leitner, D. M.; Havenith, M. *Proceedings of the National Academy of Sciences of the United States of America* **2006**, *103*, 12301–12306.

(58) Heyden, M.; Bruendermann, E.; Heugen, U.; Niehues, G.; Leitner, D. M.; Havenith, M. *Journal of the American Chemical Society* **2008**, *130*, 5773–5779.

(59) Paolantoni, M.; Comez, L.; Gallina, M. E.; Sassi, P.; Scarponi, F.; Fioretto, D.; Morresi, A. *Journal of Physical Chemistry B* **2009**, *113*, 7874–7878.

(60) Conrad, P.; de Pablo, J. *Journal of Physical Chemistry A* **1999**, *103*, 4049–4055.

(61) Engelsen, S. B.; Monteiro, C.; de Penhoat, C. H.; Perez, S. *Biophysical Chemistry* **2001**, *93*, 103–127.

(62) Naidoo, K.; Kuttel, M. *Journal of Computational Chemistry* **2001**, *22*, 445–456.

(63) Naidoo, K.; Chen, J. *Molecular Physics* **2003**, *101*, 2687–2694.

(64) Lee, S.; Debenedetti, P.; Errington, J. *Journal of Chemical Physics* **2005**, *122*, 204511.

(65) Kuttel, M. M.; Naidoo, K. J. *Carbohydrate Research* **2005**, *340*, 875–879.

(66) Kuttel, M. M.; Naidoo, K. J. *Journal of Physical Chemistry B* **2005**, *109*, 7468–7474.

(67) Choi, Y.; Cho, K.; Jeong, K.; Jung, S. *Carbohydrate Research* **2006**, *341*, 1020–1028.

(68) Phillips, J. C.; Braun, R.; Wang, W.; Gumbart, J.; Tajkhorshid, E.; Villa, E.; Chipot, C.; Skeel, R. D.; Kale, L.; Schulten, K. *Journal of Computational Chemistry* **2005**, *26*, 1781–1802.

(69) Berendsen, H. J. C.; Grigera, J. R.; Straatsma, T. P. *Journal of Physical Chemistry* **1987**, *91*, 6269–6271.

(70) Kirschner, K. N.; Yongye, A. B.; Tschampel, S. M.; Gonzalez-Outeirino, J.; Daniels, C. R.; Foley, B. L.; Woods, R. J. *Journal Of Computational Chemistry* **2008**, *29*, 622–655.

(71) Humphrey, W.; Dalke, A.; Schulten, K. *Journal of Molecular Graphics* **1996**, *14*, 33–38.

(72) Tielrooij, K.-J.; Hunger, J.; Buchner, R.; Bonn, M.; Bakker, H. J. *Journal of the American Chemical Society* **2010**, *132*, 15671–15678.

(73) Campen, R. K.; Verde, A. V.; Kubicki, J. D. *Journal of Physical Chemistry B* **2007**, *111*, 13775–13785.

(74) Stillinger, F. H. *Journal of Solution Chemistry* **1973**, *2*, 141–158.

(75) Pratt, L. R.; Chandler, D. *Journal of Chemical Physics* **1977**, *67*, 3683–3704.

(76) Lum, K.; Chandler, D.; Weeks, J. *Journal of Physical Chemistry B* **1999**, *103*, 4570–4577.

(77) Wallqvist, A.; Berne, B. *Journal of Physical Chemistry* **1995**, *99*, 2893–2899.

(78) Huang, D.; Chandler, D. *Journal of Physical Chemistry B* **2002**, *106*, 2047–2053.

(79) Athawale, M. V.; Jamadagni, S. N.; Garde, S. *Journal of Chemical Physics* **2009**, *131*, 115102.

(80) Pizzitutti, F.; Marchi, M.; Sterpone, F.; Rossky, P. J. *Journal of Physical Chemistry B* **2007**, *111*, 7584–7590.

(81) Jana, B.; Pal, S.; Bagchi, B. *Journal of Physical Chemistry B* **2008**, *112*, 9112–9117.

(82) At times less than ≈ 0.5 ps the calculated rotational anisotropy is dominated by librational motion. Capturing the response at this time scale has been demonstrated to be important when comparing simulation to experimental approaches, such as NMR, that give the integrated time correlation function.[28] Because we are here interested principally in longer time behavior and because the rotational response is non-exponential from 0-0.5 ps, the exponential fits whose time constants are shown in Figure 3 all reflect rotational anisotropies beyond 0.5 ps.

(83) These functions are calculated by binning the O$\cdots$O distance and O-H$\cdots$O angle over all configurations before a hydrogen bond between any two water molecules breaks irrevocably.

(84) Strumpfer, J.; Naidoo, K. J. *Journal of Computational Chemistry* **2010**, *31*, 308–316.

(85) Smith, B. J.; Swanton, D. J.; Pople, J. A.; Schaefer, H. F.; Radom, L. *Journal of Chemical Physics* **1990**, *92*, 1240–1247.

(86) Stirnemann, G.; Rossky, P. J.; Hynes, J. T.; Laage, D. *Faraday Discusscussions* **2010**, *146*, 263–281.

(87) Ivanov, E. N. *Soviet Physics JETP* **1964**, *18*, 1041–1045.

(88) For all averaged changes in θ, $O_d \cdots O_o$ and $O_d \cdots O_n$ we defined time zero as the first frame in which the angle θ was zero. Because, in some fraction of trajectories there are librations during the jump, this criteria results in a slight asymmetry in distances and θ around the jump event. As discussed above, the decay of the rotational anisotropy is dominated by the long time behavior so we have ignored loss of rotational correlation in the first 0.5 ps when extracting time constants. In that spirit we also calculate the $\Delta\theta$ for each jump in such a manner as to avoid this asymmetry: we take the difference of the average value of θ in $-0.4 < t < -0.2$ ps and $+0.5 < t < 1$ ps regions. Tests of different criteria found that different averaging windows do not affect our quantitative conclusions.

(89) Points with $\tau < 0.5$ were excluded from the fit because rotational motion at these time scales is dominated by libration and does not contribute significantly to the decay of the anisotropy. Points with $\tau > 13$ ps were excluded because of the large uncertainty associated with them.

(90) Frenkel, D.; Smit, B. *Understanding molecular simulation - from algorithms to applications*, 2nd ed.; Academic press: London, UK, 2002; Vol. 1.

(91) We emphasize that the SPC/E water model gives a very overstructured O-O rdf: the first peak of the O-O rdf for bulk SPC/E water has a height of 3, whereas the height from experiment is 2.2-2.3.[98–101] As such our conclusions from the free energy differences based on SPC/E rdfs hold because the work presented here uses exclusively the SPC/E water model. The actual values of free energy differences based on rdfs are not transferable to studies using other water models.

(92) Debenedetti, P. G. *Journal of Physics-condensed Matter* **2003**, *15*, R1669–R1726.

(93) Bosio, L.; Teixeira, J.; Stanley, H. E. *Physical Review Letters* **1981**, *46*, 597–600.

(94) Frauenfelder, H.; Fenimore, P.; McMahon, B. *Biophysical Chemistry* **2002**, *98*, 35–48.

(95) Frauenfelder, H.; Fenimore, P. W.; Chen, G.; McMahon, B. H. *Proceedings of the National Academy of Sciences of the United States of America* **2006**, *103*, 15469–15472.

(96) Khodadadi, S.; Roh, J. H.; Kisliuk, A.; Mamontov, E.; Tyagi, M.; Woodson, S. A.; Briber, R. M.; Sokolov, A. P. *Biophysical Journal* **2010**, *98*, 1321–1326.

(97) We note that the SPC/E water model used in our simulations does not include polarization effects, so we cannot exclude the possibility that the length scale of hydrogen bond perturbation near polar solutes is actually larger than what we observe. Simulations using polarizable water models are necessary to investigate if this is so.

(98) Leetmaa, M.; Wikfeldt, K. T.; Ljungberg, M. P.; Odelius, M.; Swenson, J.; Nilsson, A.; Pettersson, L. G. M. *Journal of Chemical Physics* **2008**, *129*, 084502.

(99) Fu, L.; Bienenstock, A.; Brennan, S. *Journal of Chemical Physics* **2009**, *131*, 234702.

(100) Neuefeind, J.; Benmore, C. J.; Weber, J. K. R.; Paschek, D. *Molecular Physics* **2011**, *109*, 279–288.

(101) Soper, A. K. *Journal of Physics-condensed Matter* **2007**, *19*, 335206.

Graphical TOC Entry